Advances in Water Resources 34 (2011) 62–82

Contents lists available at ScienceDirect

Advances in Water Resources

journal homepage: www.elsevier.com/locate/advwatres

Numerical modeling of formation damage by two-phase particulate transport processes during CO_2 injection in deep heterogeneous porous media

M.A. Sbai *, M. Azaroual

BRGM, Water Division, Groundwater and Geochemistry Modeling Group, 3, Avenue Claude-Guillemin, BP 36009, 45060 Orléans Cedex 2, France

ARTICLE INFO

Article history:
Received 16 May 2010
Received in revised form 15 September 2010
Accepted 20 September 2010
Available online 25 September 2010

Keywords:
CO_2 injection
Fines migration
Injectivity decline
Formation damage
Two-phase flow
Reservoir simulation

ABSTRACT

Prediction of CO_2 injection performance in deep subsurface porous media relies on the ability of the well to maintain high flow rates of carbon dioxide during several decades typically without fracturing the host formation or damaging the well. Dynamics of solid particulate suspensions in permeable media are recognized as one major factor leading to injection well plugging in sandstones. The invading supercritical liquid-like fluid can contain exogenous fine suspensions or endogenous particles generated *in situ* by physical and chemical interactions or hydrodynamic release mechanisms. Suspended solids can plug the pores possibly leading to formation damage and permeability reduction in the vicinity of the injector. In this study we developed a finite volume simulator to predict the injectivity decline near CO_2 injection wells and also for production wells in the context of enhanced oil recovery. The numerical model solves a system of two coupled sets of finite volume equations corresponding to the pressure–saturation two-phase flow, and a second subsystem of solute and particle convection–diffusion equations. Particle transport equations are subject to mechanistic rate laws of colloidal, hydrodynamic release from pore surfaces, blocking in pore bodies and pore throats, and interphase particle transfer. The model was validated against available laboratory experiments at the core scale. Example results reveal that lower CO_2 residual saturation and formation porosity enhance CO_2-wet particle mobility and clogging around sinks and production wells. We conclude from more realistic simulations with heterogeneous permeability spanning several orders of magnitude that the control mode of mobilization, capture of particles, and permeability reduction processes strongly depends on the type of permeability distribution and connectivity between injection and production wells.

1. Introduction

It is well established nowadays that carbon dioxide (CO_2) storage in deep geological formations (e.g. saline aquifers, depleted gas and oil reservoirs, and coal beds) is a promising measure for mitigating the impacts of climate change [41]. CO_2 injection is an extreme operation as the expected average flow rate of injection is very high because the number of operational wells will be limited within the framework of future storage projects. This is expected since one standard coal-fuel power plant station emits fewer million tons of CO_2 per year during its mean lifetime (e.g. 40 years) [9]. CO_2 in gaseous or supercritical forms (Sc-CO_2) modifies the geochemistry of formation waters leading to significant physical and thermodynamic disequilibrium and strong gas–fluid–rock interactions [56,46,7]. Furthermore, variable concentrations of particulate suspensions are sometimes present in the gas stream as a result of the capture process together with CO_2 and can not be completely avoided for economic reasons [91]. The injection of such fluid mixtures at high flow rates is likely to modify the porous medium microstructure by mobilizing and redepositing fine particles on the pore scale. These fast moving particles can clog the porous medium and may have a considerable impact on the intrinsic permeability of the rock.

Particles deposition and the resulting permeability reduction is a problem of great importance for many disciplines [54,77]. A variety of physical and possibly chemical processes contribute to the reduction of the permeability of the formation or the well screens during a deep injection operation. However, widely reported causes of well plugging in the literature [10,33,25] are due to (i) clogging due to precipitation of secondary mineral phases when injecting either highly acidic or alkaline solutions into 'water sensitive' formations, as encountered in the deep well injection of liquid wastes; (ii) clay swelling as a result of dilution and mixing between fluids; (iii) the mobilization of fine particles in non-consolidated sands and limestone formations around the wellbore. Other reported mechanisms in the literature include bacterial growth and biofilm development [73,74], scaling [36], the occlusion of gases, and the fluids emulsification [83].

* Corresponding author. Tel.: +33 2 38 64 35 27; fax: +33 2 38 64 34 46.
E-mail addresses: a.sbai@brgm.fr (M.A. Sbai), m.azaroual@brgm.fr (M. Azaroual).

0309-1708/$ - see front matter © 2010 Elsevier Ltd. All rights reserved.
doi:10.1016/j.advwatres.2010.09.009

Nomenclature

c	compressibility ($M^{-1}L\,T^2$)
C_s	salt concentration in aqueous solution (mole L^{-3})
C	mass concentration of fine particles ($M\,L^{-3}$)
$\mathbf{D}_s$	solute hydrodynamic dispersion tensor in aqueous solution ($L^2\,T^{-1}$)
D	diffusion coefficient ($L^2\,T^{-1}$)
d	mean diameter (L)
fe	flow efficiency factor (−)
f	fractional flow function (−)
g	z-axis component of the gravity vector $\mathbf{g} = (0,0,g)^T$ ($L\,T^{-2}$)
H	heaviside function (−)
Iw	well index (−)
$\mathbf{K}$	rock intrinsic permeability tensor (L^2)
k_{rl}	relative permeability of fluid phase l (−)
k_B	Boltzmann's constant (J/K)
m	empirical exponent parameter (−)
n	power law of the reduced permeability–porosity relationship (−)
p	fluid pressure ($M\,L^{-1}\,T^{-2}$)
q	total injection/withdrawal source/sink term ($M\,L^{-3}\,T^{-1}$)
R_{sa}	salt adsorption rate on porous media surfaces (mole $L^{-3}\,T^{-1}$)
R	particles rate term ($M\,L^{-3}\,T^{-1}$)
rw	well radius (L)
S	fluid saturation (−)
s	skin factor (−)
t	time (T)
T	temperature (°)
$\mathbf{u}$	fluid velocity vector ($L\,T^{-1}$)
z	vertical axis component (L)

Greek letters

α	rate constant
γ	rate of change of the filtration coefficient ($M^{-1}\,L^3$)
κ	parameter depending on the residual permeability of the plugged pores (−)
λ	fluid mobility ($M^{-1}\,L^3\,T$)
μ	fluid viscosity ($M\,L^{-1}\,T^{-1}$)
ρ	fluid density ($M\,L^{-3}$)
σ	mass of particles deposited over pore walls per unit bulk volume ($M\,L^{-3}$)
σ^*	mass of particles trapped at pore throats per unit bulk volume ($M\,L^{-3}$)
ϕ	rock porosity (−)
Δ	difference operator (−)
θ	angle (rad)
Θ	correction function for high concentration suspensions
Γ	computational domain boundary
Ω	computational domain

Subscripts

0	initial value
bh	bottomhole
c	CO_2 phase, or capillary
cp	CO_2 wet particles
f	fine particles
fe	flow efficiency
i	particle type index
ip	intermediately wet particles
I	interface zone between CO_2 and water
o	oil phase
op	oil particle
l	fluid phase index
lc	critical quantity in fluid phase l
p	particle
s	salt
t	total
w	water phase
wp	water wet particles
lr	residual in phase l

Superscripts

cl	colloidally released
d	deposition
h	hydrodynamically released
max	maximum
p	pore throat
t	phase transfer
T	vector transpose
$*$	effective parameter value

Mobilization of fines in natural porous media is exhibited by chemical and hydrodynamic perturbations at the pore scale. Previous field observations demonstrated the occurrence of chemical perturbations by changes in ionic strength [37], pH increase in the injected aqueous solution composition [80], the chemical composition of injected surfactants [1], and the infiltration of organic matter [69]. The so-called hydrodynamic effect [60] has been observed in different situations when increasing the groundwater seepage velocity. Common situations are injection with high flow rates, rapid infiltration in the unsaturated zone of the subsurface [45], and rapid flow dynamics in fractured media [29]. In the context of deep CO_2 injection other release mechanisms are expected, such as release of metal oxides (i.e. hematite) from corroded metal pipes [26]. The hematite particles are strongly positively charged and therefore, will be attracted by the ubiquitous negatively charged quartz grains in sandstones [5,34]. Rapid injectivity decline due to permeability decrease will follow as the pore pressure increases. At some level, the fluid cannot be injected anymore into the damaged formation with the targeted high flow rates until the permeability is restored by other physical or chemical processes [58]. In general, clogging due to fines release, migration, and capture is an irreversible process. Once formation damage has occurred, initial petrophysical properties are unlikely to be completely restored by subsequent remediation.

Well impairment has several consequences such as the risk of uncontrolled rise of cap-rock pore pressure above the admissible fracturing pressure, initiation and propagation of fractures [36], and hence developing preferential flow paths for CO_2 leakage. In extreme cases, injection wells have to be abandoned. Therefore, comprehensive understanding of the effects of fine migration on formation damage is important for planning, design, and maintenance steps of carbon dioxide disposal projects in deep geological formations. Know-how from experimental characterization and field investigations related to the role of particulate transport processes within aqueous fluids in the subsurface lead to question on the performance of CO_2 injection when endogenous or exogenous fine particles are mobilized in porous media.

Demonstrated evidence of cake formation close to the wellbore environment and following injectivity difficulties during industrial operations of enhanced oil recovery (EOR), geothermal fluids reinjection, and deep disposal of hazardous industrial wastes have been reported by several authors. In the offshore Siri oil field at

the southern Persian Gulf, water injection started in 1984 with a rate of 9100 bbl/day, but was stopped in 1990 due to a rapid injectivity decline when the rate had dropped to 2200 bbl/day [55]. A faster decline was observed in five wells at the Gulf of Mexico field [79]. Water injection rate declined from 7000 bbl/day to less than 1000 bbl/day in just 200 days. In these two cases the particles in injected water were filtered up to 10 μm, yet the decline was very severe. Boisdet et al. [17] noted an injectivity decline from 85 to 30 m^3/h, and a wellhead pressure increase from 4 to 5 MPa, during one year of injection in a geothermal brine doublet producing a sandstone Triassic formation (Paris basin). Suspended particles in the injected fluid were identified as the principal cause of injectivity decline in all the above cases. The severity of injectivity decline is case-dependent. It is related to particle sizes, solid concentrations, reservoir properties, and ionic strength and/or pH of the carrying fluid. Therefore, comprehensive understanding of physicochemical processes controlling carbon dioxide injectivity is an important issue for a successful injection operation in sandstone formations.

As far as it goes, only few papers address the issues related to mathematical and numerical modeling aspects of two-phase particulate transport phenomena. EOR applications from the reservoir engineering literature are notoriously the main target of previously published results and mostly assume a single-phase flow near the well. In CO_2 sequestration science, still in its infancy, this paper is the first tackling the problem from CO_2–EOR and storage perspectives. Recently reported experimental studies from reactive percolation of CO_2 enriched brine or Sc-CO_2 demonstrated the occurrence of many *in situ* particle generation stages in the process of secondary mineral precipitation. These particles do not only move within the Sc-CO_2 phase but they exhibit an important volume growth within time. Shao et al. [76] reported a progressive growth of particulate matter from nanoparticles formed only after 5 h to aggregates after 22 h. They quantitatively noted four orders of magnitude volume growth, of the aggregates, after 159 h.

Despite the extensive research on particle capture mechanisms in porous media that has been conducted in the previous decades, complete understanding of the process is still limited in many ways. For instance, most reservoir simulation models cannot quantify precisely the formation damage close to the well (at the cell containing the injection well). Most often, they only allow to specify, a priori, a skin factor around the wellbore zone to account for this damage. Several authors [84,85] (and references therein) provided computational procedures to evaluate the half-life as a measure of injection performance of an injection well from laboratory-derived data. Pang and Sharma [63] have predicted the injectivity decline in wells with various types of completions such as perforated, gravel packed, and fractured wells. In these theoretical models, experimental data parameters of the mass filtration process are determined at the laboratory scale, and directly used in Darcy-scale models to predict injection well performance. Formation damage due to fines transport by fluid flow is typically modeled as a mass filtration process.

The main objectives of this paper is to develop, verify, and test on available experimental data, a general framework for predicting injectivity decline by particulate transport processes in two-phase flow systems. The numerical model is applied on example problems during CO_2 injection in heterogeneous reservoirs. To the best of our knowledge, no generic numerical codes capable of simulating mechanistically all these processes are available.

The remainder of this paper is organized as follows. In Section 2 a phenomenological formation damage model accounting for two-phase particle release, mobilization, and capture mechanisms is presented. Next, model verifications on experimental data are provided to demonstrate the numerical code capability to describe the physics of given problems. In Section 5, demonstrative model applications on generic site scale oil reservoirs and saline aquifers are presented to show potential applications, and simulate the injectivity decline near injection and production wells. The last subsection preceding the concluding remarks discusses how this work could be improved in the framework of future CO_2 storage projects.

2. Phenomenological model description

The mathematical equations are based on the global pressure and phase saturation formulation to predict spatial distribution of the pressure, phase velocities, and the non-wetting phase (i.e. CO_2) saturation. These are complemented by a solute transport equation in the aqueous phase for calculating the spatial distribution of the solute mass which may trigger the salinity-induced mobilization of *in situ* colloidal fines. Particle transport processes are described through a set of coupled convection–diffusion equations for each subset of particles. The couplings occur only over quasi-linear rate laws for basic processes of release from pores bodies, mobility in fluid phases, and capture in pores throats. Because of data limitations and computational requirements, grouping of particles in this work is assumed to depend mainly on their surface wettability for multiphase processes [53]. Quantitative assessment of the permeability decline is strongly dependent on the accuracy of experimental data on permeability–porosity relationships. We briefly discuss the limitations of existing formulations in the literature and approximate relationships used in the following numerical simulations.

2.1. Two-phase flow of CO_2 and water phases

Two-phase fluid flow equations are based on the global formulation which is proved to be more computationally efficient than other approaches, i.e. two-pressure or phase pressure formulations [23]. We consider here the isothermal two-phase fluid flow motion equation for the global pressure, p, of two immiscible fluids [22,39]:

$$\phi c_t \frac{\partial p}{\partial t} = \nabla \cdot [\mathbf{K}\lambda_t(\nabla p - (f_w\rho_w + f_c\rho_c)g\nabla z)] + \frac{q_w}{\rho_w} + \frac{q_c}{\rho_c}, \quad (1)$$

where c_t is the total compressibility of the two fluids and rock system, ϕ is the rock porosity, p is the fluid pressure, $\lambda_t = \lambda_w + \lambda_c$ is the total mobility, $\lambda_l = \frac{k_{rl}}{\mu_l}$ is the relative permeability, k_{rl}, of phase $l = (w,c)$ to its viscosity, μ_l, ratio; $\mathbf{K}$ is the principal intrinsic permeability of the porous medium, ρ_l is the density of fluid phase l, $f_l = \frac{\lambda_l}{\lambda_t}$ is the fractional flow function of phase l, q_l is a time-dependent total injection/withdrawal term of phase l, $\nabla = \left(\frac{\partial}{\partial x}, \frac{\partial}{\partial y}, \frac{\partial}{\partial z}\right)$ is the partial differential operator, t is time, and g is the z-axis component of the gravity vector $\mathbf{g} = (0, 0, -g)^T$ directed downward. Moreover, the total compressibility is the sum of the individual compressibility to the rock, and saturation weighted compressibilities of water, c_w, and CO_2, c_c, such that $c_t = \frac{1}{\phi}\frac{d\phi}{dp} + S_w c_w + S_c c_c$.

Denoting the carbon dioxide phase saturation by S_c, Eq. (1) is supplemented with a non-linear diffusion-convection like saturation equation for the CO_2 phase and usually known as the Buckley–Leverett equation with gravity, given as follows:

$$\phi\frac{\partial S_c}{\partial t} = -\nabla \cdot [f_c\mathbf{u} - \mathbf{K}f_c\lambda_w\Delta\rho g\nabla z] + \frac{q_c}{\rho_c} - S_c\frac{\partial\phi}{\partial t}, \quad (2)$$

where $\mathbf{u} = \mathbf{u}_w + \mathbf{u}_c$ is the total fluid flow velocity, and $\Delta\rho = \rho_w - \rho_c$ is the difference between densities of the aqueous and CO_2 phases respectively. Since variations in porosity by the presented model are expected to be small, the last term in the right hand side of Eq. (2) is dropped in the adopted space–time discretization schemes.

Pressure and saturation Eqs. (1) and (2) must be supplemented with other closure and constitutive constraints such as

$$\sum_{l=w,c} S_l = 1, \tag{3}$$

$$k_{rl} = f(S_w). \tag{4}$$

Several functional forms of phase relative permeability, k_{rl}, as a function of water saturation, S_w, are proposed in the literature. In this study, we use the general form provided by Eq. (5) for the relative permeability functions:

$$k_{rl} = k_{rl}^0 (S_l^*)^{m_l} \quad l = w, c, \tag{5}$$

where $S_l^* = \frac{S_l - S_{lr}}{1 - S_{cr} - S_{wr}}$ is the normalized l-phase saturation, k_{rl}^0 is the end-point relative permeability of phase l, S_{lr} is the residual saturation of phase l, and m_l is an empirical exponent parameter for phase l which depends on the grain-size distribution.

Note that since we neglect the capillary pressure effects on the spatial distribution of the saturation, the global pressure is given as

$$p = p_w = p_c. \tag{6}$$

The total fluid flow velocity dependence on the global pressure is given as follows (for more details see [23]):

$$\mathbf{u} = -\mathbf{K}\lambda_t(\nabla p - (\rho_w f_w + \rho_c f_c) g \nabla z). \tag{7}$$

A numerical solution is uniquely defined for Eqs. (1) and (2) subject to relationships defined by Eqs. (5) and (7) by appropriately setting additional initial and boundary conditions as shown in Section 2.5.

2.2. Governing equations for particulate processes

2.2.1. Salt transport

Solute transport in porous media is governed by processes like water advection, mechanical dispersion, and surface adsorption [11]. The governing equation for the transport of a salt specie, s, in the aqueous phase is

$$\phi S_w \frac{\partial C_s}{\partial t} + \nabla \cdot (\mathbf{u}_w C_s - \phi S_w \mathbf{D}_s \cdot \nabla C_s) + R_{sa} + Q_s = 0, \tag{8}$$

where C_s is the mass concentration of salt ions s, $\mathbf{D}_s$ is the hydrodynamic dispersion tensor of salt s accounting for the respective contributions from mechanical dispersion and molecular diffusion, R_{sa} is the adsorption rate of salt ions on pore surfaces, and Q_s is the rate of salt ions change caused by a source/sink contribution.

2.2.2. Transport of particles

When exogenous particles are injected into a porous medium, together with CO_2, a fraction is attracted to the surfaces of pore walls whenever the electrostatic forces acting between them exceed the hydrodynamic and gravitational forces. A second fraction is trapped on the pore throats by the simultaneous effects of size exclusion and particle bridging. The remaining fraction migrates farther in the reservoir. The later includes mainly small particles of less than one micron and for which Brownian diffusion is likely to take place. Particles are either hydrophobic (cp), hydrophilic (wp), or have an intermediate wettability behavior (ip). Therefore, hydrophobic particles exist only in the rich CO_2 phase, hydrophilic particles exist in the aqueous phase, and particles of intermediate wettability remain in the interface zone, I, between the two phases. All particles enumerated so far can undergo mass transfer between fluid phases. An exception are colloidal fines denoted by f which exist exclusively in the aqueous phase. Particle transport in porous media is governed by a linear convection–diffusion mass conservation equation as (see [42] for experimental evidence):

$$\begin{aligned} &\phi S_l \frac{\partial C_{il}}{\partial t} + \nabla \cdot (\mathbf{u}_l C_{il} - \phi S_l D_{il}^* \nabla C_{il}) + R_{il} + Q_{il} = 0, \\ &i = wp, cp, f; \quad l = w, c, \end{aligned} \tag{9}$$

where C_{il} is the mass concentration of particles i in fluid phase l, D_{il}^* is the effective diffusion coefficient of particles i in fluid phase l, R_{il} is the net rate of loss of particle species i in fluid phase l and which are deposited in pore surfaces and pore throats, and Q_{il} is the rate of change of particle volume belonging to a source/sink term.

Intermediately wet particles tend to be located at the interface between the two liquid phases and their movement have been shown to be restricted to the interface zone [57]. The continuity equation for such particles is

$$\phi \frac{\partial C_{ip}}{\partial t} + \nabla \cdot \left(\mathbf{u} C_{ip} - \phi D_{ip}^* \nabla C_{ip} \right) + R_{ip} = 0, \tag{10}$$

where C_{ip} is the mass concentration of intermediately wet particles in the interface zone, and R_{ip} is the net rate of loss of intermediate particles at the interface.

2.2.3. Rate laws for particulate transport processes

From the literature review given above, individual mechanistic processes that contribute to particles rate in Eq. (9) are fines release by (i) colloidal or (ii) hydrodynamic forces, (iii) particle deposition on pore surfaces, (iv) particle capture by pore throats, and (v) inter-phase mass transfer of particles. Therefore, the rate equation takes the following general form:

$$R_{il} = R_{il}^{cl} + R_{il}^{h} + R_{il}^{d} + R_{il}^{p} + R_{il}^{t}, \quad i = wp, cp, f, ip, \tag{11}$$

where R_{il}^{cl} and R_{il}^{h} are release rates of particle species i from pore walls wet with fluid phase l by colloidal or hydrodynamic forces respectively, R_{il}^{d} is the deposition rate of particle species i on pore surfaces wet with fluid phase l, R_{il}^{p} is the capture rate of particle species i on pore throats filled with fluid phase l, and R_{il}^{t} is the rate of particle species i displaced from fluid phase l to the other phase or to the intermediate zone in-between and vice versa.

The rates of colloidally and hydrodynamically induced mobilization of *in situ* fines and other particles, respectively, in sandstones are first-order decay equations [47,90] as in the following expressions:

$$R_{fw}^{cl} = -\alpha_{fw}^{cl} \sigma_{fw} H(C_{sc} - C_s) \tag{12}$$

$$R_{il}^{h} = -\alpha_{il}^{h} \sigma_{il} H(\|\mathbf{u}_l\| - \|\mathbf{u}_{lc}\|), \tag{13}$$

$$(i = wp, cp, f;\ l = w, c) \quad (i = ip;\ l = I)$$

where σ_{fw} is the mass of fines per unit fluid volume available at pore bodies and H is the Heaviside function. Eq. (12) means that colloidal release of fines is limited by a critical salinity threshold, C_{sc}, above which colloidal forces between pore walls and fines change from being repulsive to an attractive state. Notice that for all other particles, R_{iw}^{cl} is always equal to zero because only fines could be released by colloidal forces. Likewise, Eq. (13) is an expression of the hydrodynamic effect observed for particles mobilization where $\mathbf{u}_{lc}$, is the critical velocity of fluid phase l, above which release from pore surfaces occurs, and below which this individual mechanism becomes ineffective.

Following Gruesbeck and Collins [38] the rate of deposition of water and CO_2-wet particles in pore walls of the same wettability is a generalization of the equation first proposed by Iwasaki [42] in aqueous single-phase flow:

$$\begin{aligned} &R_{il}^{d} = \alpha_{il}^{d} \|\mathbf{u}_l\| C_{il} \\ &i = wp, l = w \quad i = cp, l = c \end{aligned} \tag{14}$$

where α_{il}^{d} is a parameter known as the filtration coefficient of particle species i in fluid phase l. This coefficient is determined from time series of suspended particle effluent concentration measured

in laboratory coreflood tests [2]. For dilute suspensions, it is generally admitted that the filtration coefficient is independent of particle concentration and could be calculated from the pressure drop along the core [40,30,12,27]. However, for highly concentrated particulate suspensions the filtration coefficient is seldom constant [90] meaning that the deposition rate is not a simple linear function of the fluid velocity as Eq. (14) expresses. In the latter case, other non-linear relationships between the filtration coefficient and the mass of deposited particles, σ^d, have been suggested by several authors. For instance, Saripalli et al. [70] used the following equation:

$$\alpha^d = \alpha_0^d(1 + \gamma\sigma^d), \tag{15}$$

where γ is the rate of increase or decrease of the filtration coefficient whose typical values are difficult to obtain theoretically and are only determined through inversion of effluent concentration of suspended particles. The determination of the coefficient of filtration, which is critical for a realistic prediction of the injectivity decline, is described in much more detail in the literature [78,62,89,25]. Alvarez et al. [3] has developed an inverse computational procedure to deduce the filtration coefficient and formation damage as functionals and not constant coefficients. They suggest their recovery from measurements of the time series of suspended particle effluent concentration and of pressure drop along the core involving a double inverse problem.

For instance, recent evidence suggests that filtration of microorganisms in saturated porous media may not be consistent with the first-order kinetic Eq. (14) where exponential decrease in mobile particle concentration with travel distance is expected. Tufenkji et al. [81] attributed this behavior to the heterogeneity in the interactions between microbial particles and sediment grains, and incorporated it by including a probability distribution function for the filtration coefficient. The review [82] (and references therein) on recent developments specific to the transport of microbial particles may be consulted by the interested reader. In our work we do not consider details specific to microbiologically mediated particles and this topic shall not be discussed further in the remainder of this paper.

Particle capture at the pore throats by blocking and bridging is the only mechanism that can occur for all types of particles enumerated so far ($i = wp, cp, ip, f$). Thus, it is expected that its individual impact will be more significant under two-phase flow conditions. The capture rate of particles at pore throats is assumed to be proportional to the particle mass flux, that is

$$R_{il}^p = \alpha_{il}^p \|\mathbf{u}_l\| C_{il}; \quad i = wp, cp; \quad l = w, c, \tag{16}$$

$$R_{fw}^p = \alpha_{fw}^p \|\mathbf{u}_w\| C_{fw}, \tag{17}$$

$$R_{ip,l}^p = \alpha_{ip,l}^p \|\mathbf{u}\| C_{ip,l}, \tag{18}$$

Interphase transfer of particles cannot take place in all directions. Water-wet particles migrate from CO_2-rich phase to the water phase, while CO_2-wet particles flow from the water phase to CO_2 liquid, and finally particles of intermediate wettability could move from the primary two phases to the interface zone in-between. For these three possibilities the rate equations are identical to those given by Ku and Henry [50], and Liu and Civan [53].

2.2.4. Brownian diffusion of particles

The Brownian diffusion coefficient, D_{il}, for dilute suspensions of spheres, is given by the Stokes–Einstein equation:

$$D_{il} = \frac{k_B T}{3\pi\mu_l d_p}, \tag{19}$$

where d_p is the mean-size particle diameter, k_B is the Boltzmann's constant, and T is the absolute system temperature.

The Stokes–Einstein equation for Brownian diffusion is valid only for low particulate concentrations. For higher concentrations the equation must be adjusted as suggested by [67]:

$$D_{il} = \frac{k_B T}{3\pi\mu_l d_p \Theta(C_{il})}, \tag{20}$$

where $\Theta(C_{il})$ is a correction factor for high concentrations of particulate suspensions. In those cases, we use the empirical relation obtained by [28]:

$$\Theta(C_{il}) = (1 - C_{il})^{-6.55}. \tag{21}$$

2.2.5. Effective diffusion coefficient of fine particles

The effective diffusion coefficient D_{il}^* is estimated for an idealized bed in which the sphere centers are randomly distributed in space. Weissberg [88] derives an upper bound for the effective diffusion coefficient applicable to spheres of uniform or non-uniform sizes:

$$D_{il}^* = \frac{\phi D_{il}}{1 - \frac{1}{2}\ln\phi}. \tag{22}$$

2.3. Permeability–Porosity relationships

The accuracy of formation damage prediction depends on the ability of empirical permeability–porosity correlations to capture the geometric details of pore size distribution, pore shape, and connectivity [32]. The Kozeny–Carman (KC) approach [49,20], widely used and discussed in the literature, requires some means of estimating the specific surface, which can be problematic [16]. It is also known that this model, although fairly accurate for unconsolidated sands, tends to become unreliable for consolidated sandstones. Schlueter [75] examined the error incurred by the KC hydraulic radius theory for different pore shapes. Her results indicate that for geometrically regular pores the hydraulic radius approximation provide little confidence for accurate estimation of the actual rock permeability. It is obvious that no simple general correlation between porosity and permeability can be applied to all rock types. On the other hand, dynamic correlations or models that consider porous media undergoing alteration due to fluid–rock interactions during formation damage are more useful for formation damage prediction than their static counterparts. Verma and Pruess [87] state that differences in the porosity–permeability relationships are not only related to differences in pore parameters discussed above but also to the different mechanisms of porosity change. Mechanisms such as mineral precipitation, and capture of particles (by blocking and bridging) at pore throats may strongly affect these narrow portions of pores, and are therefore, much more effective as vehicles for formation damage. A complete review of previously published approaches pertaining to permeability prediction in the context of particulate transport processes has been given by Civan (e.g. [25, Chapter 5]) and will not be repeated in this paper. In the following subsection, only those used so far in the presented numerical simulations of this paper are briefly discussed.

By introducing the fines plugging effect in the original KC equation, Liu and Civan [53] and later Ju et al. [44] have expressed the instantaneous permeability change by release and retention of particles as

$$\frac{K}{K_0} = \left((1 - fe)\kappa + fe\frac{\phi}{\phi_0}\right)^n, \tag{23}$$

where κ is a parameter accounting for the residual permeability of the plugged formation enabling therefore the so-called gate or valve effect of the pore throats, whereby $K = 0$ even if $\phi \neq 0$, n is an index

which is claimed to be in the range between 2.5 and 3.5 by Ju et al. [44], and *fe* is a flow efficiency factor expressing the fraction of unplugged pores available for flow given as

$$fe = 1 - \sum_i \left(\alpha_{fe,i} \sum_l \sigma^*_{il} \right), \tag{24}$$

where $\alpha_{fe,i}$ is the coefficient of flow efficiency for particles *i*.

We further define σ_{il} and σ^*_{il} as the mass of particles per unit fluid volume deposited at the pore bodies and pore throats of the porous medium respectively, and such that:

$$\frac{\partial \sigma_{il}}{\partial t} = R^{cl}_{il} + R^{h}_{il} + R^{d}_{il}, \tag{25}$$

$$\frac{\partial \sigma^*_{il}}{\partial t} = R^{p}_{il}. \tag{26}$$

By denoting σ_{il0} and σ^*_{il0} the respective mass of these quantities per bulk fluid volume at initial time, it becomes possible to estimate the change in porosity due to all particulate processes previously discussed in this paper as

$$\phi = \phi_0 - \sum \Delta\phi \tag{27}$$

$$\sum \Delta\phi = \left(\sum \sigma_{il} + \sum \sigma^*_{il} - \sigma_{il0} - \sigma^*_{il0} \right) \Big/ \rho_p \tag{28}$$

where ρ_p is the density of particulate suspensions. Notice that the time-dependent porosity change, $\Delta\phi$, includes release and retention mechanisms simultaneously. Thus, it becomes positive if retention mechanisms are dominant leading to permeability damage, and negative when the release mechanisms dominate leading to a permeability enhancement.

2.4. Well modeling

Numerical solution of two-phase flow equations of a reservoir requires an additional relationship between the grid-block pressure and the wellbore pressure through an appropriate well index. A well model calculates its injectivity or productivity index in a numerical, semi-analytical, or pure analytical procedure. We use a Peaceman finite difference model [23] considering expressions for rate-controlled injection/production wells, and production wells controlled by a prescribed bottom-hole pressure. Vertical and horizontal well completions are allowed in any direction of the cartesian grid. The extra set of constraints that need to be undertaken for multiphase flow in anisotropic media are as follows:

$$q_l = Iw \frac{\rho_l k_{rl}}{\mu_l} (p - p_{bh} - \rho_l (z_{bh} - z)). \tag{29}$$

Following Peaceman [65] for a vertical well parallel to the *z*-axis:

$$Iw = \frac{\theta \sqrt{k_x k_y} \Delta z}{\ln(r^*/rw) + s}, \tag{30}$$

$$r^* = 0.28 \frac{(k_y/k_x)^{1/2} \Delta x^2 + (k_x/k_y)^{1/2} \Delta y^2}{(k_y/k_x)^{1/4} + (k_x/k_y)^{1/4}}, \tag{31}$$

while for an horizontal well parallel to the *x*-axis

$$Iw = \frac{\theta \sqrt{k_y k_z} \Delta x}{\ln(r^*/rw) + s}, \tag{32}$$

$$r^* = 0.28 \frac{(k_z/k_y)^{1/2} \Delta y^2 + (k_y/k_z)^{1/2} \Delta z^2}{(k_z/k_y)^{1/4} + (k_y/k_z)^{1/4}}, \tag{33}$$

where q_l is the well flow rate for phase $l = (w, c)$, *Iw* is the well index, p_{bh} is the bottom-hole pressure, z_{bh} is the well datum level depth, *z* is depth, r^* is the effective radius, *rw* is the radius of the well, θ is the angle open to flow, $\mathbf{K} = diag(k_x, k_y, k_z)$ is the grid-block anisotropic permeability, and *s* the skin factor resulting from initial formation damage caused by drilling. Depending upon what is specified, either the bottom-hole pressure p_{bh} or the flow rate q_l end up as extra unknowns per completion in the resulting linear system.

2.5. Boundary and initial conditions

Let Γ be the boundary of the computational domain Ω, where Γ_{pD} and Γ_{pN} are non-overlapping Dirichlet and Neumann boundaries for the pressure equation, respectively. The pressure equation is subject to the following boundary conditions:

$$p_l = p_D \quad \text{on } \Gamma_{pD} \quad l = w, c, \tag{34}$$

$$\mathbf{u}.\mathbf{n} = q_N \quad \text{on } \Gamma_{pN}. \tag{35}$$

The saturation equation is subject to boundary conditions:

$$\mathbf{u}_c \cdot \mathbf{n} = q_N \quad \text{on } \Gamma_{sN}, \tag{36}$$

where $\mathbf{n}$ denotes the outward unit normal, q_N is the imposed volumetric injection rate at the Neumann boundaries, and Γ_{sN} is the Neumann boundary for the saturation equation. Our numerical model allow for any combination of the boundary conditions for the global pressure and saturation equations.

Since in situ particles are only generated inside the porous medium, a zero flux condition apply to external inlet boundaries and injection wells in Eq. (9):

$$\nabla C_{fw} = 0 \quad \text{on } \Gamma_{cN}, \tag{37}$$

where Γ_{cN} represents the set of external Neumann boundaries for the particle convection–diffusion equation. For externally introduced particles the boundary condition is

$$C_{il} = C_{il,in} \quad \text{on } \Gamma_{cD}, \tag{38}$$

where $C_{il,in}$ is the concentration of externally introduced *i* particles in the injected fluid phase *l*, and Γ_{cD} represents the set of external Dirichlet boundaries for particle concentrations. Likewise the boundary condition for intermediately wet particles governed by Eq. (10) is

$$\nabla C_{ip} = 0 \quad \text{on } \Gamma_{cN}. \tag{39}$$

Eq. (8) is subject to Cauchy and Neumann type boundary conditions as given below:

$$\mathbf{u}_w C_s - \phi S_w \mathbf{D}_s \nabla C_s = \mathbf{u}_{w,in} C_{s,in} \quad \text{on } \Gamma_{scC} \tag{40}$$

$$\nabla C_s = 0 \quad \text{on } \Gamma_{scN} \tag{41}$$

where Γ_{scC} and Γ_{scN} are non-overlapping domain boundaries of the third type or Cauchy and Neumann types for the solute concentration equation, respectively. $\mathbf{u}_{w,in}$ is the injection velocity, and $C_{s,in}$ is the salt concentration of the injected water phase.

The presented governing equations are additionally subject to the following set of initial conditions:

$$p = p_0(\mathbf{x}), \tag{42}$$

$$S_c = S_{c,0}(\mathbf{x}), \tag{43}$$

$$C_{il} = 0 \quad \forall\, i, l, \tag{44}$$

$$C_{ip} = 0, \tag{45}$$

$$C_s = C_{s,0}(\mathbf{x}), \tag{46}$$

$$\sigma_{fw} = \sigma_{fw,0}(\mathbf{x}), \tag{47}$$

$$\sigma^*_{fw} = 0, \tag{48}$$

$$\sigma_{il} = 0; \quad i = cp, l = c; \quad i = wp, l = w, \tag{49}$$

$$\sigma^*_{ip,l} = 0. \tag{50}$$

where $p_0(\mathbf{x})$ is the initial space distributed pressure, $S_{c,0}(\mathbf{x})$ is the initial distribution of saturation, and $C_{s,0}(\mathbf{x})$ is the initial distribution of salt concentration.

2.6. Model approximations

Our conceptual model should be viewed as a first step towards a much sophisticated coupling methodology between two-phase flow and particulate transport processes as it would occur in engineering practice. Currently identified model limitations are given below.

(1) The isothermal two-phase flow model is based on the global pressure formulation which is known to hold only for incompressible to slightly compressible fluids [22,23]. This assumption is not valid for the full range of representative temperature and pressure conditions in deep saline aquifers targeted by CO_2 storage. This is especially the case for shallow sedimentary basins. The new non-iterative fractional flow formulation introduced recently by Amaziane and Jurak [4] for compressible two-phase flow problems is a possible extension in this direction.
(2) The relative permeability and capillary pressure curves may exhibit strong hysteretic profiles, along many scanning curve pathways, when CO_2 injection design involves drainage and imbibition simultaneously. Previous studies demonstrated the importance of these mechanisms to the length and extension of the CO_2 plume and to capillary trapping mechanism as well [31]. Implementation and discussion of these processes in the framework of our model are left to future tasks. This would enable a better insight into the impact of variable flow rate and injection fluids on the clogging magnitude close to the injection well. Since there exist only very few published data emphasizing brine-CO_2 systems [13–15,66], more experimental research studies in this direction are recommended.
(3) The relative permeability and capillary pressure curves are assumed to be time-independent. This is not realistic since the particles deposited in pore surfaces change the wettability properties of the rock and the set of particles deposited in pore throat capillaries could break the interfacial tension between the two fluids. Although this was observed experimentally for nanoparticle polysilicon solids [43], this issue is not yet fully resolved in the literature and needs additional theoretical and experimental investigations. Combining pore scale models of two-phase flow [86] and particulate transport [61] augmented with laboratory work may prove useful for a better understanding of these processes.
(4) Geochemical reactions are not taken into account which precludes the presented model to simulate fluctuating absolute permeability changes as was observed in some carbonate rocks [59]. This is the case, for instance, when some secondary precipitating mineral phases in pore throats could undergo dissolution latter which could reopen partially, completely, or even enlarge the previously clogged pore space.
(5) Geomechanical poroelastic effects leading to possible initiation of fractures and their growth when the pores are sufficiently clogged [35] are neglected by this simulation model.

3. Numerical solution procedure

Numerical solution of Eqs. (1)–(33), subject to initial and boundary condition Eqs. (34)–(50), simultaneously is very complex since many nonlinear dependencies are involved, and particulate transport equations are coupled to many rate ordinary differential equations. A fully coupled solution of all equations would be a daunting task. An efficient solution strategy should focus on identification of subsystems that are weakly coupled to each other to enable sequential splitting, and possibly different spatial discretization and time stepping techniques for each subset of governing equations.

First, the global pressure and CO_2 phase saturation Eqs. (1) and (2), subject to initial and boundary conditions, are solved using standard techniques commonly used in reservoir engineering [8,52]. To this end, we implemented two different strategies in our simulator. First, an IMPES like scheme [8] is preferred for one-dimensional problems dominated by viscous forces. This is the case for advection controlled experiments and when accurate tracking of the saturation fronts nearby injection and production wells is sought. However, the main drawback of this scheme is the limiting Courant–Friedreichs-Lewy (CFL) time step requirement enforced for stability. At the field scale, this constraint is often much demanding and hampers the global solution efficiency since CFL numbers in the computational domain can vary by orders of magnitude [48]. In practical cases, we devise the use of an implicit solver for the saturation equation that is unconditionally stable [8]. The pressure solver is a fully implicit Euler in time and first-order upwind finite-volume in space [52]. For structured grids this scheme is equivalent to the standard two-point flux approximation scheme (TPFA), and to the widespread cell-centered finite difference scheme for rectangular grids. The saturation equation is solved either fully implicitly or with a mixed iterative scheme combining a nonlinear explicit solver for the viscous and gravity-driven terms and a nonlinear implicit solver for the capillary diffusion term. A robust Newton–Raphson adaptive procedure [64] combined with line-search techniques is employed to solve the underlying nonlinear systems resulting from the saturation equation.

This first step of the entire algorithm determines cell centered saturations and the global fluid pressure. Velocity components are given at cells edges along the three orthogonal directions of the grid. Next, phase velocities are substituted from the total velocity (see [23] for more details) as they are needed for transport of each group of particles in the respective fluid phase:

$$\mathbf{u}_w = f_w\mathbf{u} + \mathbf{K}\lambda_c f_w(\rho_w - \rho_c)g\nabla z, \tag{51}$$

$$\mathbf{u}_c = f_c\mathbf{u} + \mathbf{K}\lambda_w f_c(\rho_c - \rho_w)g\nabla z. \tag{52}$$

The advection–dispersion Eq. (8) followed by particles transport Eqs. (9) and (10) are solved by splitting techniques. The advection term is solved by an explicit first-order upwind finite-volume technique. The intermediate concentrations fields are next substituted to the dispersion-diffusion equations systems which are solved implicitly. Unlike for the solute transport equation, particulate transport equations are subject to different rate constants related to release, mobilization, surface deposition, and pore-throats blocking as discussed in previous paragraphs. To estimate the mass of flowing particles, the rate equations are implicitly integrated from initial concentrations fields resulting from the diffusive step by the DASPK computer package [18]. Finally, it becomes affordable to estimate particles rates in a post-processing stage such that masses of each particle class deposited in pore bodies or throats are determined. Notice that, particulate transport equations are processed sequentially since they are independent on each other. This computational task lends itself naturally to parallel processing if one is dealing with a large number of particle classes. Before jumping to the next time step, the final step in the overall algorithm estimates the permeability loss or gain in each grid cell by using one of the two presented concepts relating permeability and porosity changes.

The numerical model allows for different time steps in the pressure–saturation and convection–diffusion subsystems. However, no efforts have been undertaken to optimize or automate this process. In the sequential solution of the pressure saturation equations convergence is achieved when the residual of the

Newton–Raphson iteration is smaller than a prescribed tolerance value. We follow a sequential non-iterative solution approach (SNIA) for the numerical solution of the particulate transport equations in all demonstrative example problems discussed in this paper. Numerical solution by this technique was compared with alternative techniques based on a sequential iterative technique (SIA) and found to be quantitatively similar. This inter-comparison study will be pursued and presented in a forthcoming paper.

4. Model verification and testing at the laboratory scale

The literature on experimental data for the class of problems being discussed in this paper is very scarce. As such, there is no reported measurements of Sc-CO_2 injection with exogenous particles, or combined to any other mechanism, as discussed above, triggering in situ fines transport. Although, we are aware of a number of similar experiments guided recently, they focus more on reporting the nature of salt deposits rather than measuring particles transport along the sampled cores. For the numerical code verification in this paper, we make use of the data set previously published by Sarkar [71], Sarkar and Sharma [72] and which was also a subject of an earlier simulation work by Liu and Civan [53]. Although the data set is not specifically suited for Sc-CO_2-brine systems, it provides a necessary first level benchmark to proxy other two-phase flow systems. Successful verifications enable to establish confidence on the accuracy of the numerical implementation and the code capability to tackle realistic engineering grade problems.

4.1. Single-phase flow experiments

The first model verification is based on laboratory experiments conducted by Sarkar and Sharma [72] on two core samples. The first experiment involves freshwater injection into a Berea sandstone core saturated with 3% chloride sodium brine. The second experiment was conducted on a similar core sample but only with the presence of a residual oil phase. Core data for these two samples are reproduced in Table 1. Other simulation data, such as the rates of particulate processes, dispersion coefficient of the solute, and so on, are reported in Table 2 and are identical to those given by Liu and Civan [53] following their history match with experimental data. It seems from previous interpretations of these experiments in the literature that hydrodynamic release of fines does not take place here due to the low injection flow rate. However, fines mobilization is mainly due to the salinity gradient when flushing the interstitial brine with freshwater.

The two simulations predict processes of in situ fines release from pore surfaces, migration, and capture by pore throats as depicted in Fig. 1 at the core outlet position. These three mechanisms occur simultaneously in the narrow lifetime of the fines concentration wave, which equals 33 and 42 min for the two simulations

Table 1
Berea sandstone core data given by [72] for single-phase flow experiments.

Property	Experiment 1	Experiment 2
Core diameter (cm)	2.54	2.54
Core length (cm)	8.30	8.30
Initial porosity	0.21	0.21
Initial permeability (darcies)	0.0654	0.0825
Fines density (g/cc)	2.50	2.50
Residual oil saturation	0.00	0.367
Initial brine salinity (mol/cc)	0.51	0.51
Injection flow rate (cm/s)	4.31×10^{-4}	4.31×10^{-4}
Freshwater/brine viscosity (cp)	1.0	1.0
Core outlet pressure (atm)	1.0	1.0

Table 2
Solute transport and particulate rate data used for simulating in situ fines migration experiments presented by [53].

Property	Experiment 1	Experiment 2
σ_{fw0} (g/cc)	0.025	0.02
C_{sc} (mol/cc)	7×10^{-3}	7×10^{-3}
D (cm^2/s)	1×10^{-4}	1×10^{-4}
α_{fw}^{cl} (s cc/mol)	0.435	0.280
α_{fw}^{p} (cm^{-1})	5.25	5.25
$\alpha_{fe,f}$ (cc/g)	35.4	35.4
κ_f	0.0	0.0
n	3	3

respectively. It is clear that with presence of the residual oil phase concentration waves of the solute species (Fig. 2(b)) and particles (Fig. 1(b)) are retarded within the same factor due to a lower mobility of the flowing phase. Another fundamental difference with the presence of residual oil is a lower constant rate of fines release (see Table 2) than in the case where the core is saturated with brine. This is likely related to the lower pore surface exposed to the flowing phase in the second experiment and results in a lower fines concentration maximal value and pore surfaces/throats plateau in the second experiment (see Fig. 1(b) and Fig. 2(b)). In both cases, the total porosity reduction does not exceed 1%. However, this little porosity change leads to a rapid permeability impairment as shown in Fig. 3 for both experiments. Simulated and measured permeability damage at the Berea cores inlet are compared resulting in a satisfactory agreement. In the first experiment, without residual oil, it is concluded that permeability impairment is the most severe with a reduction over almost three orders of magnitude. In the second experiment, a lower permeability reduction is again related to the lower mass of mobilized fines and the subsequent lower capability to plug pore throats.

4.2. Two-phase flow experiment

In-situ fines mobilization and migration is investigated under simultaneous two-phase flow of oil and water. Experimental data are provided by Sarkar [71] on a Berea sandstone core similar to those used previously. The data used in this simulation are provided in Table (3). Model parameters are identical to data given in Table (2) for the second experiment, except for the initial mass of fines, σ_{fw0}, which is taken equal to 0.0188 g/cc. Furthermore, to be consistent with other works [53] that simulated this third experiment on the Berea sandstone core, we use curve fitted parameters, m_l and k_{rl}^0, for relative permeabilities of oil and brine respectively according to Eq. (5). Fitted parameters are $k_{rw}^0 = 0.03$, $k_{ro}^0 = 0.84$, $m_w = 1.75$, and $m_o = 3.25$ (see Fig. 4).

We point out that capillary pressure effects are neglected in this simulation, and since the model is one-dimensional, gravity-driven migration or buoyancy of the water phase is also neglected. Then, water saturation Eq. (2) becomes equivalent to the well-known Buckley–Leverett equation [19] in this third simulation experiment.

Results of this third simulation are also in close agreement with Liu and Civan [53] conclusion that formation damage and fines migration under two-phase flow conditions, neglecting the capillary pressure, are similar to those of the second experiment considering only residual oil. Fig. 5(a) confirm the above made observation, although pore surfaces and throats concentrations plateaux are slightly on a lower level. This conclusion is due to the first fact that fines in water are not being allowed to be transferred to the oil phase and plug oil–wet pore throats, and second to the rapid breakthrough of freshwater saturation as shown in Fig. 5(b). The last observation suggests also that fines migration

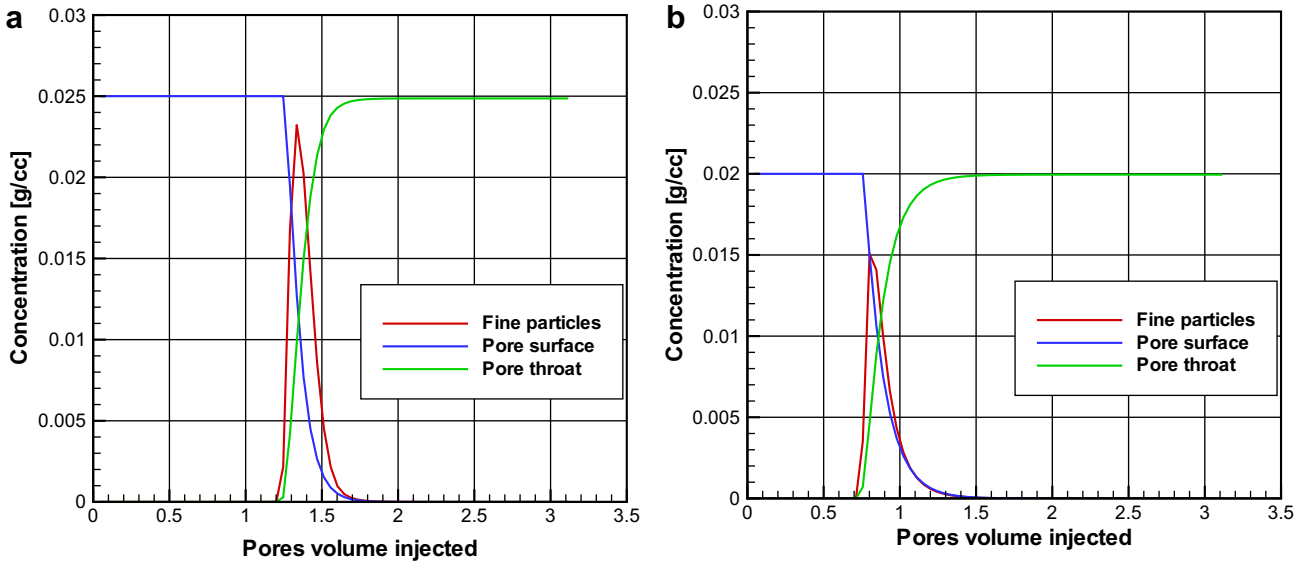

Fig. 1. Simulated effluent pore surface, pore throat, and particles fines concentrations for (a) experiment 1 and (b) experiment 2 flushing NaCl brine in Berea cores with freshwater. Experiments belong to cores without and with residual oil, respectively.

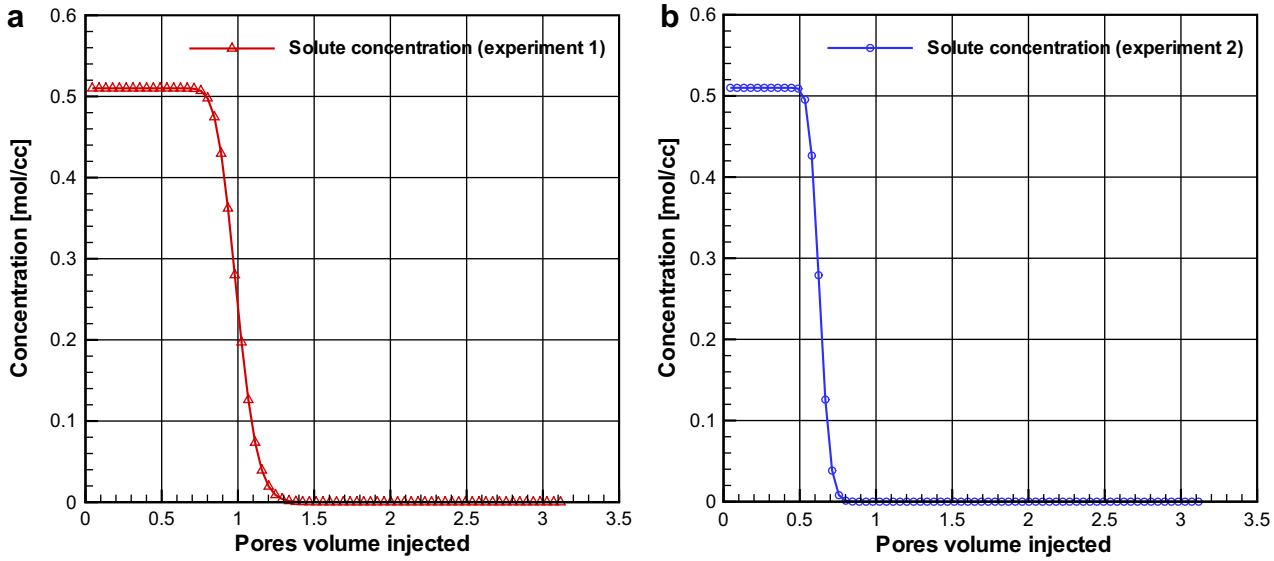

Fig. 2. Simulated effluent solute concentration for (a) experiment 1 and (b) experiment 2 flushing NaCl brine in Berea cores with freshwater. Experiments belong to cores without and with residual oil, respectively.

inside the core is dependent on the shape of the relative permeability curves of the flowing fluids.

5. Model applications to CO_2 injectivity at the field scale

In the previous section our model was checked against available experimental laboratory data to establish confidence in the implemented numerical solution method and the relevance of the integrated mechanisms. Simulation at the core scale is a prerequisite for comprehensive understanding of the interplay between formation damage processes occurring in the laboratory, but cannot be directly applied at the field scale. In practical applications, the velocity field around the wellbore is radial and rapidly decreasing but not linear, which may change the time scales of basic processes like particle release, migration, and capture, leading to different space and time evolution of the permeability close to the well. In the framework of EOR by CO_2 flooding fluid flow dynamics are complex due to simultaneous operation of many injection and production wells. Furthermore, the type of reservoir heterogeneity, connectivity, and channeling, may significantly affect the geometry and relative position of the damaged area. These issues will be investigated by several numerical experiments as discussed in next paragraphs.

5.1. The five-spot well problem

In this first example, the aqueous phase is pumped out from a 3000 m deep reservoir through four square corner's wells with an equal injection rate. CO_2 phase is injected from a well at the center of the domain with a total injection flow rate of 1.15×10^6 tons/y. The reservoir geometry, production data, as well as the parameters for fines mobilization are given in Table 4.

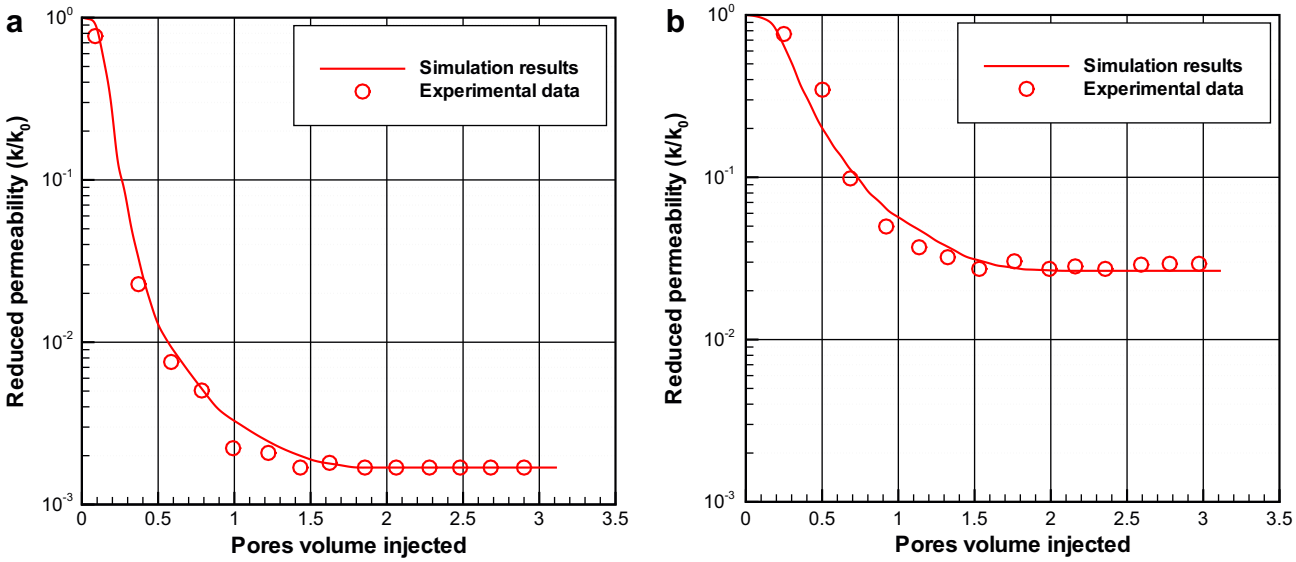

Fig. 3. Comparison between simulated and experimental measurement data of reduced permeability at the inlet of Berea cores for (a) experiment 1 and (b) experiment 2 flushing NaCl brine with freshwater. Experiments belong to cores without and with residual oil respectively.

Table 3
Berea sandstone core data given by [71] for the two-phase flow experiment.

Property	Experiment 3
Core diameter (cm)	2.53
Core length (cm)	8.27
Initial porosity	0.209
Initial permeability (darcies)	0.122
Fines density (g/cc)	2.50
Residual oil saturation	0.30
Connate water saturation	0.27
Initial brine salinity (mol/cc)	0.51
Injection flow rate (cm/s)	3.78×10^{-4}
Freshwater/brine viscosity (cp)	1.0
Oil viscosity (cp)	22.9
Core outlet pressure (atm)	1.0

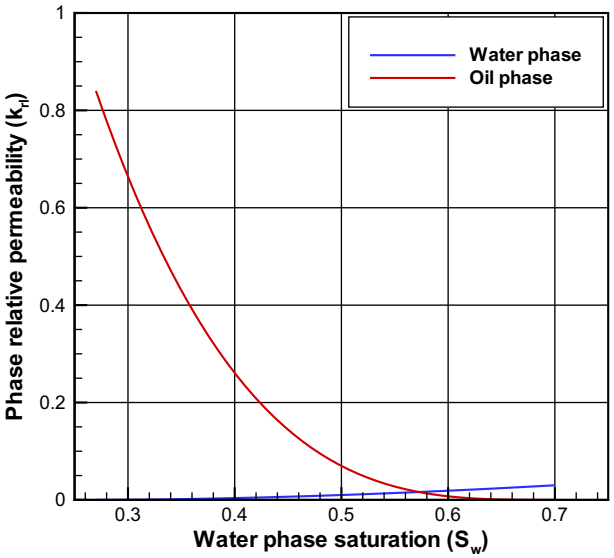

Fig. 4. Relative permeability curves for Berea core used in experiment 3 for two-phase flush of NaCl brine and oil with freshwater (after Liu and Civan [53]).

In all simulation scenarios discussed further, salinity-induced mobilization is not taken into account by the Sc-CO_2-wet particles considered herein since there is an uncertainty as to the relevance and importance of this mechanism with a supercritical liquid-like CO_2 fluid. A constant global time step of 1 day is selected throughout, while internal particle kinetics sub-time steps are automatically selected by the numerical integration package.

Fig. 6 shows the results obtained after a period of injection amounting to one month. Particles are released by hydrodynamic injection forces, from the circular zone where the CO_2 fluid phase velocity exceeds its prescribed critical value. This behavior is observed in the very early days of simulation as the concentration of the suspended particles rises sharply in all cells neighboring the injection well. Mobile concentration rapidly stabilizes in this region as demonstrated in Fig. 7(a). A fast rate of surface capture is observed for cells close to the injector and therefore only excess mobile solid matter is allowed to move along the flow pathlines and to be captured later in deeper surface sites. This behavior is illustrated by surface concentrations in Fig. 7(a) and (b) belonging to cells whose centers are located at 4.95 and 49.5 m of radial distance from the injection well respectively. Competition between release and surface capture processes occurs at the same time but at different space positions where the latter is retarded in space. This behavior is explained by the dispersive nature of the surface capture process whereas the release mechanism is sharper (see Fig. 6(B) and (C)). It has been verified that the former conclusive fact is not due to numerical dispersion artifacts by selecting an explicit solver for the saturation and concentrations equations. Outside the zone markedly impacted by particles migration, surface deposition in pore surfaces is smaller in magnitude and controlled exclusively by Brownian diffusion. Particle diffusion is an important mechanism for particles of size less than one micron, implying a higher effective diffusion coefficient than used in our simulation. Such effects could be readily introduced in the general framework of our simulator by adding other classes of CO_2-wet particles of different sizes owing to different particulate rates and effective diffusion coefficients. But, since diffusion-controlled capture mechanisms have only a secondary impact on a short time basis, they could be safely neglected for the simulations presented. A permeability decrease of more than 20% is observed nearby the injection well. The radius of the most clogged area is quite small following sharply the distribution of concentrated fines in pore throats. Particle bridging and blocking processes are always

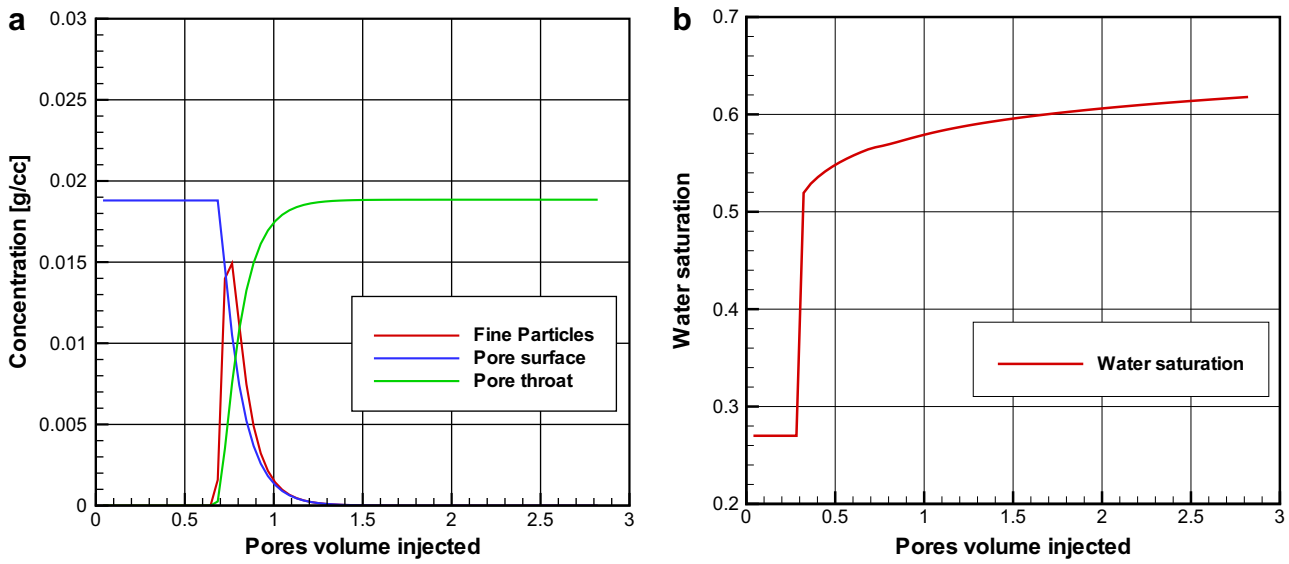

Fig. 5. Simulated (a) effluent pore surface, pore throat, particles fines concentrations, (b) and freshwater breakthrough for two-phase flow experiment in Berea core when flushing NaCl brine with freshwater.

Table 4
Parameters used for studying CO_2 injection in five-spot well pattern.

Parameters of the geological model	Value	Parameters for fines mobilization	Value
Reservoir length (m)	500	α_{fc}^{cl} (s^{-1})	0.0
Reservoir width (m)	500	α_{fc}^{h} (m^{-1})	3.8×10^{-4}
Reservoir thickness (m)	5	α_{fc}^{d} (m^{-1})	1.2×10^{-4}
Number of FV cells	101×101	α_{fc}^{pt} (m^{-1})	6.2×10^{-6}
Initial pressure (MPa)	30	$\alpha_{fe,f}$ (m^3/kg)	0.6
Viscosity of CO_2 (mPa s)	0.077	u_{cc} (m/s)	0.2×10^{-4}
Viscosity of water (mPa s)	0.50	σ_{fc0} (kg/m^3)	0.0
Residual CO_2 saturation	0.3	ρ_p (kg/m^3)	2500
Residual water saturation	0.3		
Initial porosity	0.3		
Initial permeability (μm^2)	0.85		
Injection rate of CO_2 (m^3/h)	150		
Temperature (°C)	60		
Fluid salinity (g/l)	50		

restricted to the vicinity of the injector owing to the size exclusion effect akin to the nature of this process.

As depicted in Fig. 8 a lower residual saturation of CO_2 ($S_{rc} = 0.03$) leads to different spatial distributions of suspended and deposited solid matter. This reflects the important impact of the relative permeability type curves on particles migration and distribution in two-phase flow systems. Therefore, lower residual content of CO_2 enhances the fines mobility in the reservoir and accelerates clogging around sinks and production wells. Results obtained from another simulation with lower residual saturation of the water phase ($S_{rw} = 0.03$) as illustrated in Fig. 9 show very little impact on concentrations distributions and permeability reduction. Other sensitivity analysis simulations lead to conclude that a lower porosity, ϕ, has a similar effect on the distribution and magnitude of permeability change as a low CO_2 residual saturation. From Fig. 10 it is clear that at high porosities permeability loss is restricted to the injector, otherwise it is much dispersed in the central zone and elliptical regions at the domain corners. We noticed from results of other sets of simulations that maximal permeability change is quite insensitive to initial permeability values being varied from 1 mD up to 100 Darcy during this time frame.

Therefore, even in the absence of salinity-induced mobilization of in situ fine particles, as shown in the previous laboratory experiments [71,72], the performance of CO_2 injection at very high flow rates needs to be carefully designed to avoid rapid fines accumulation at the injection well as demonstrated in this simple numerical experiment. In this process design, such damage is not restricted to the injection well, most especially, at low reservoir porosity and low non-wetting residual phase saturation. Nevertheless, these conclusions are only valid under the simplistic assumption of medium homogeneity. The potential impact of field-scale heterogeneity is assessed in a series of simulations guided by another application example where all processes are reconsidered again with a more realistic permeability field.

5.2. CO_2 injection into an heterogeneous reservoir

In this second application example, two two-dimensional permeability maps are extracted from the full three-dimensional permeability field used by the SPE-10 comparative solution project [24]. The first map is the top layer of the Tarbert formation which is a representation of a prograding near-shore environment where the permeability is relatively smooth. The second map corresponds to the 36th layer in the Upper-Ness formation sequence where permeability is fluvial and could be characterized as a high-contrast heterogeneous porous medium. The selected layers are described

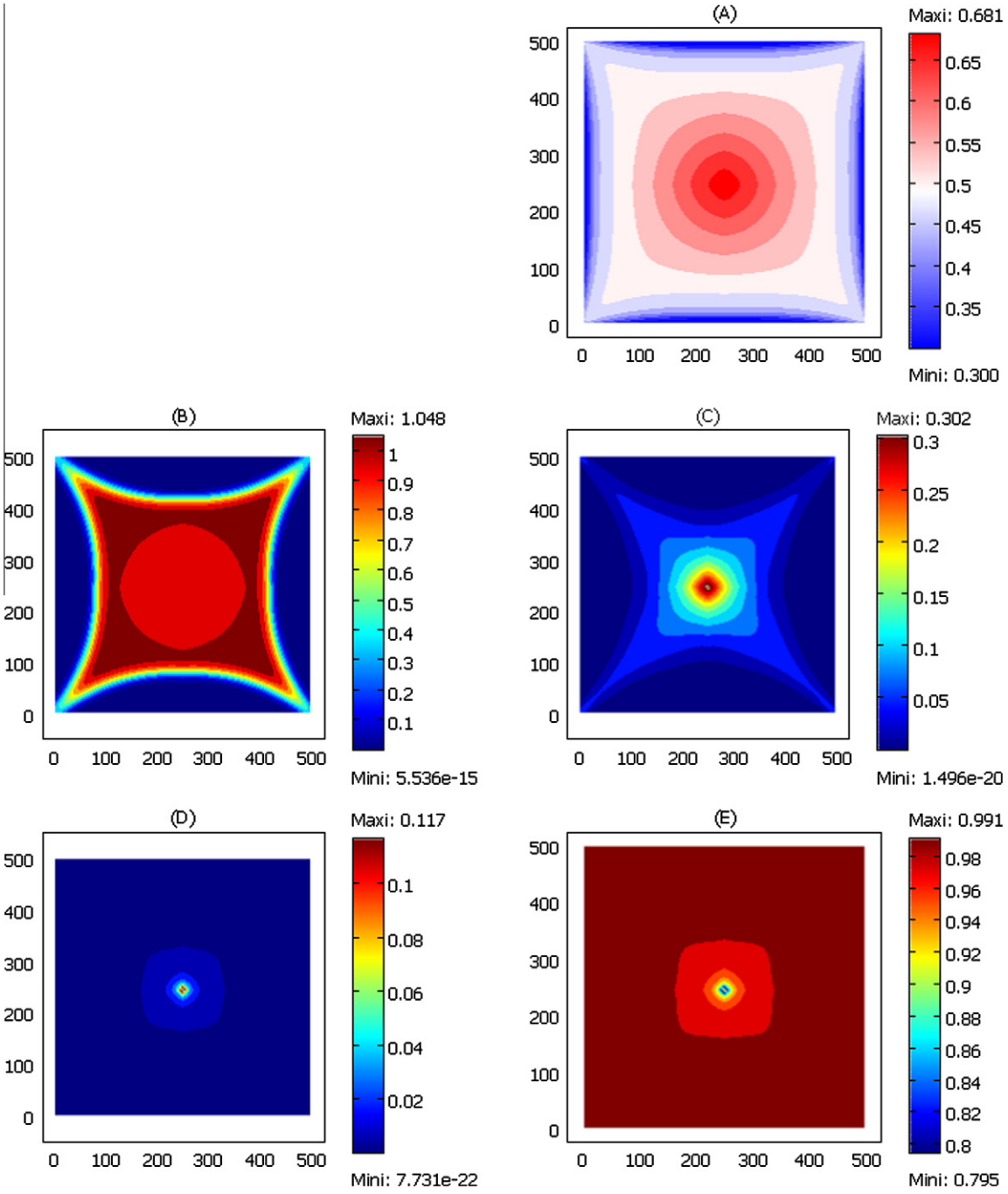

Fig. 6. Simulation results after 1 month of CO_2 injection in a five-spot well pattern – homogeneous medium – $S_{rc} = 0.3$ and $S_{rw} = 0.3$ - showing spatial distribution of (A) CO_2 phase saturation, mass concentrations of (B) suspended particles, (C) deposited particles in pore surfaces, and in (D) pore throats; and (E) the permeability reduction factor.

on a regular cartesian grid with 60×220 (13,200) cells. The porosity is strongly correlated with the horizontal permeability and contains about 2.5% null values. To avoid division by zeros in these cells, we simply replace the null values by a threshold minimal value. The reservoir parameters, production data, and other extra parameters for particle release, transport, and capture are given in Table 5. Here the oil phase is extracted from four production wells at the domain corners with an equal flow rate and CO_2 is injected into the formation from an injection well in the center.

Fig. 11 shows the numerical results obtained after 1 month of CO_2 injection into the smooth heterogeneous medium. Fig. 12 depicts the results for the same problem except the medium permeability is chosen as homogeneous and equal to the mean permeability ($k = 7.3 \times 10^{-11}$ m^2) of the first permeability map. Comparison of these results leads to the key conclusion that a heterogeneous medium exhibits more damage than an otherwise homogeneous equivalent. This is due to preferential surface capture and pore blocking processes of CO_2 particles along narrow pathlines as markedly seen in Fig. 11(D) and (E). Whereas in the homogeneous case, Fig. 12(D) indicates a more dispersive effect of the surface capture process as discussed earlier in the first example. Likewise, more particles are captured at pore throats in the heterogeneous case scenario. In the later case (Fig. 11(F)), permeability reduction is well established along a complex 'X' shaped channels and is deeper than in the homogeneous equivalent case (Fig. 12(F)).

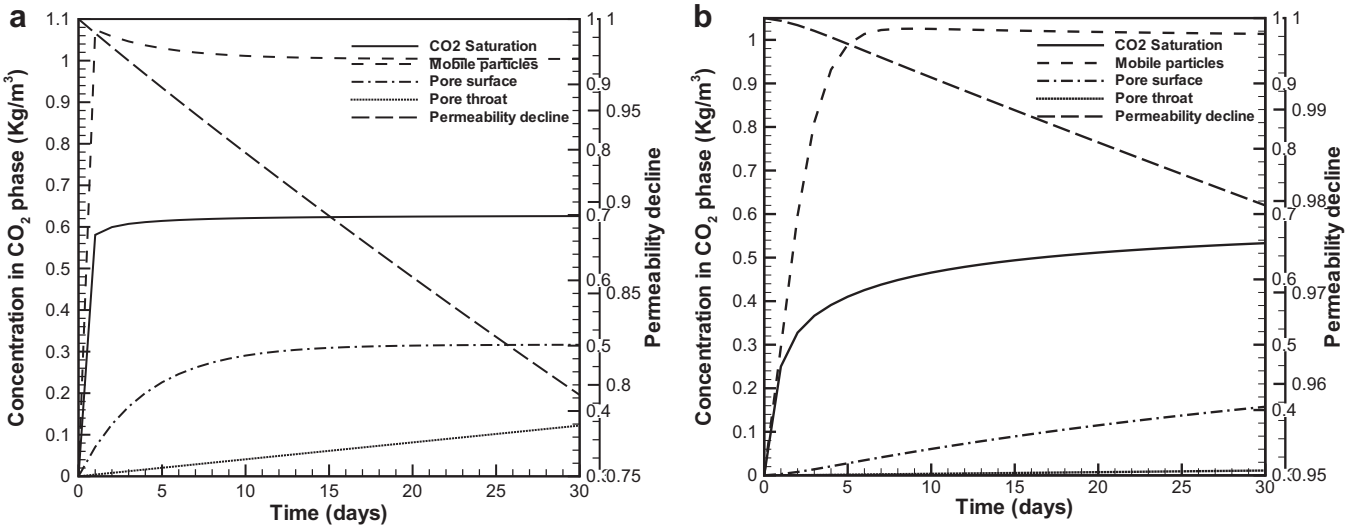

Fig. 7. Evolution of pore surface, pore throat, particles concentrations, and permeability reduction at radial distance of (a) 4.95 and (b) 49.5 m from the injection well, respectively.

In the case of fluvial permeability field, Fig. 13 show simulation results after 30 days of CO_2 injection. The injectivity decline is slightly higher due to an already well established high-permeability channel and a high contrast with its surrounding. Here the particle capture mechanisms are exclusively controlled by the medium heterogeneity and not by the hydraulic interactions as in the smooth permeability case. Indeed the narrow channel volume intercepts most of the particles at the pore surfaces (Fig. 13(D)) and pore throats (Fig. 13(E)). Additionally, we can see from Fig. 13(F) that injectivity loss distribution in the reservoir is not gradually decreasing radially from the injection well. It is not anymore restricted close to the injection well and could be reached in other parts of the reservoir, as in the most permeable channel composed from fluvial sediments, or in fragmented sets of spots at the vicinity of some production wells. The later permeability damage locations are associated with cells of smaller porosity, higher concentrations of the suspended matter, and thus higher mobility of the CO_2 fluid phase.

5.3. Discussions

In the two previous subsections, it has been demonstrated that particulate suspensions released under the unprecedented high flow rates anticipated for CO_2 storage projects could lead to formation damage not only close to the injection (and production) wells. Notice that in our simulations only the hydrodynamic release mechanism was selected. This limitation is not associated with model formulation and its numerical implementation but rather to the state of the art within Sc-CO_2-particulate suspension mixtures and their interactions with electrolytic solutions at different ionic strengths.

Injection of freshwater into brine electrolytic aqueous phase solutions triggers colloidal mobilization of fines as discussed previously. Direct extension to other injection fluids depends on their interfacial tension, wettability and chemical composition. Supercritical carbon dioxide interfacial tension and wettability is a complex function of chemical composition [51], pressure, and temperature [21]. At the current stage of knowledge, very little is known on the salinity induced release of in situ particles in presence of a supercritical CO_2 fluid. Due to the lack of experimental data, the simulations presented in this section should be viewed as a lower end-members when salinity-induced mobilization of in situ fines is neglected.

We also demonstrated that, even for the small time frame considered, permeability of other parts of the reservoir may change also which have implications not only for injectivity (and productivity) processes but also on subsequent CO_2 fluid flow dynamics and its saturation distribution. The presented simulations are comprehensive as they shed more light on the possible interactions between the basic processes and the model ability to identify key factors for formation damage and its distribution which is not otherwise possible at the laboratory. Therefore, a coupled model of two-phase flow and particulate transport equations is useful and needed for some phases of a CO_2 sequestration project. Namely in the phases of site characterization, and monitoring.

Formation damage and injectivity decline induced by mobilization of in situ particles and co-injection of a CO_2-particle mixture has not been included yet in existing risk assessment frameworks. We believe that this is due to the worldwide relatively short experience on studies of carbon sequestration mechanisms in sandstone sedimentary basins. In other environments, such as the Utsira sands in Sleipner (North Sea), the first commercial scale CO_2 injection site, little injectivity decline was observed yet. Favorable high initial permeability and porosity, and a quite probable consolidated sand materials of this formation are probably the key factors maintaining a high injectivity. This is not currently the case for other sequestration projects (i.e. Snohvit site) running into trouble because of little CO_2 storage capacity or otherwise little injectivity.[1] This will be also unlikely the case in other large sedimentary basins needed to deploy carbon storage at a commercial scale. Since spatial scale resolutions needed are in the range of several hundreds of kilometers squares, the probability that a new injection well intersects a poorly consolidated and low permeability zone could not be completely avoided. Such probability increases with the factors explained so far. A scientific based approach is therefore needed to account for such rising probability of well failure and the related project costs for site selection. Next to the initial screening phase and during site characterization, and as more data becomes available, the proposed numerical model could be used for predictive purposes to estimate the well injectivity index evolution during the project lifetime.

On a longer time basis, we expect other implications for CO_2 storage mechanisms. This requires however a more thorough study

[1] See the press news at http://www.barentsobserver.com/?id = 4757670&cat = 0&language = en. Retrieved, 2 August, 2010.

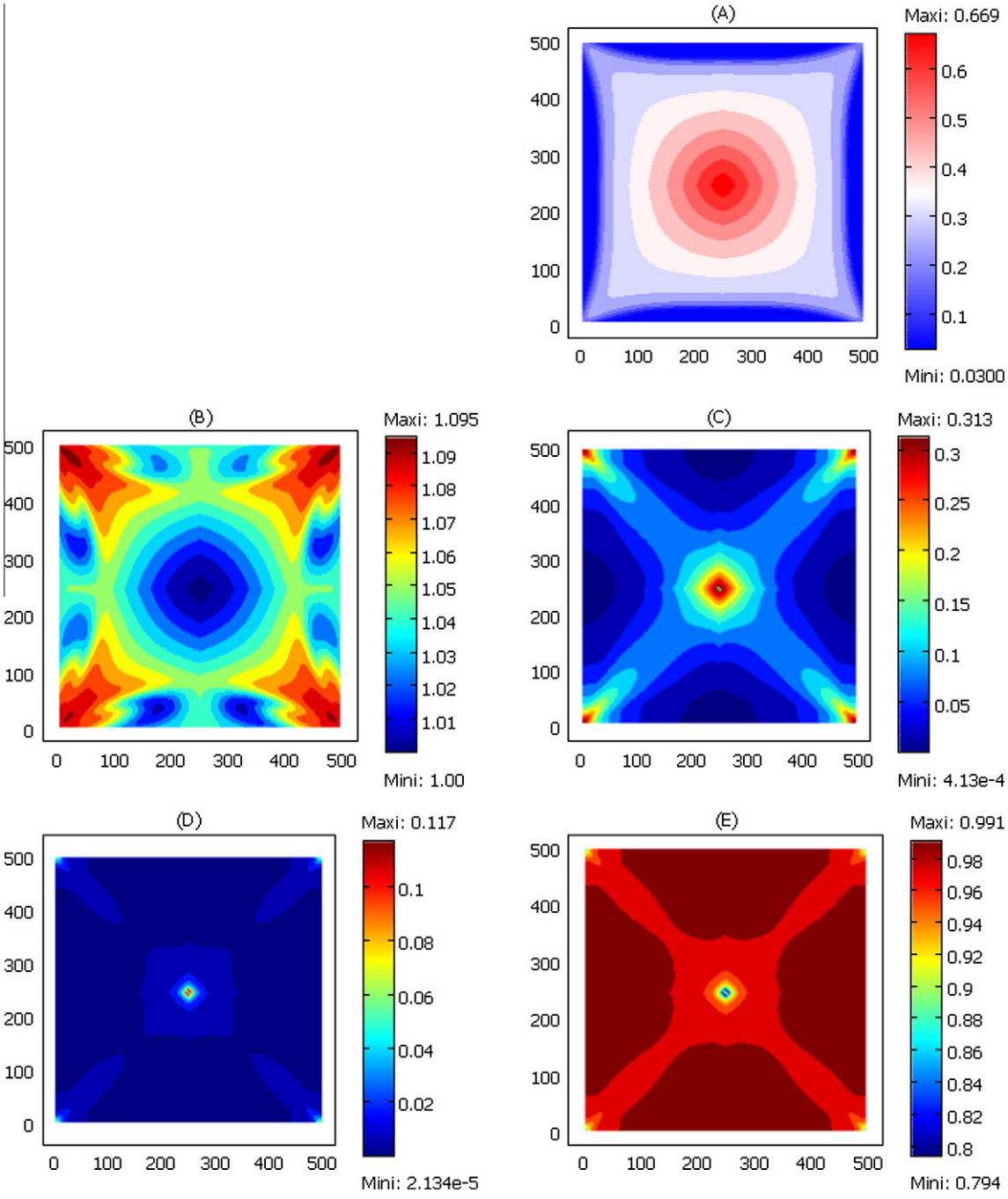

Fig. 8. Simulation results after 1 month of CO_2 injection in a five-spot well pattern – homogeneous medium – $S_{rc} = 0.03$ and $S_{rw} = 0.3$ – showing spatial distribution of (A) CO_2 phase saturation, mass concentrations of (B) suspended particles, (C) deposited particles in pore surfaces, and in (D) pore throats; and (E) the permeability reduction factor.

and constitutes another plan for our future research work. Particularly, competition between the CO_2 phase gravity override and the mechanism of particles interception by their sedimentation should be investigated and requires an extension of the presented model. Such effort is important if the exact location of formation damage along the depth of the well screens is of interest. Much detailed simulations require also more sophisticated gridding near the wellbore because as seen in the simulations above the particles capture processes are occurring over variable and different spatial scales.

We do not argue however that all particulate transport processes must be included in simulations pertaining to studies of CO_2 storage or that our simulator handle them at all. For instance, desiccation of carbonate formations associated with salt precipitations next to immobile CO_2 dissolution in the residual aqueous phase [68] is another indirect mechanism by which CO_2 wet particles will migrate due to the high flow rate of injection. Reported simulations in the literature did not include yet particle transport processes and their impact on formation damage [6,68]. Simulation of this additional mechanism is possible by the presented model through proper calibration of the hydrodynamic release rate. Other processes relevant to sandstone formations include shrinkage of clay (i.e. smectic or illitic) particles within the dry supercritical CO_2 phase and their swelling when they move into the aqueous

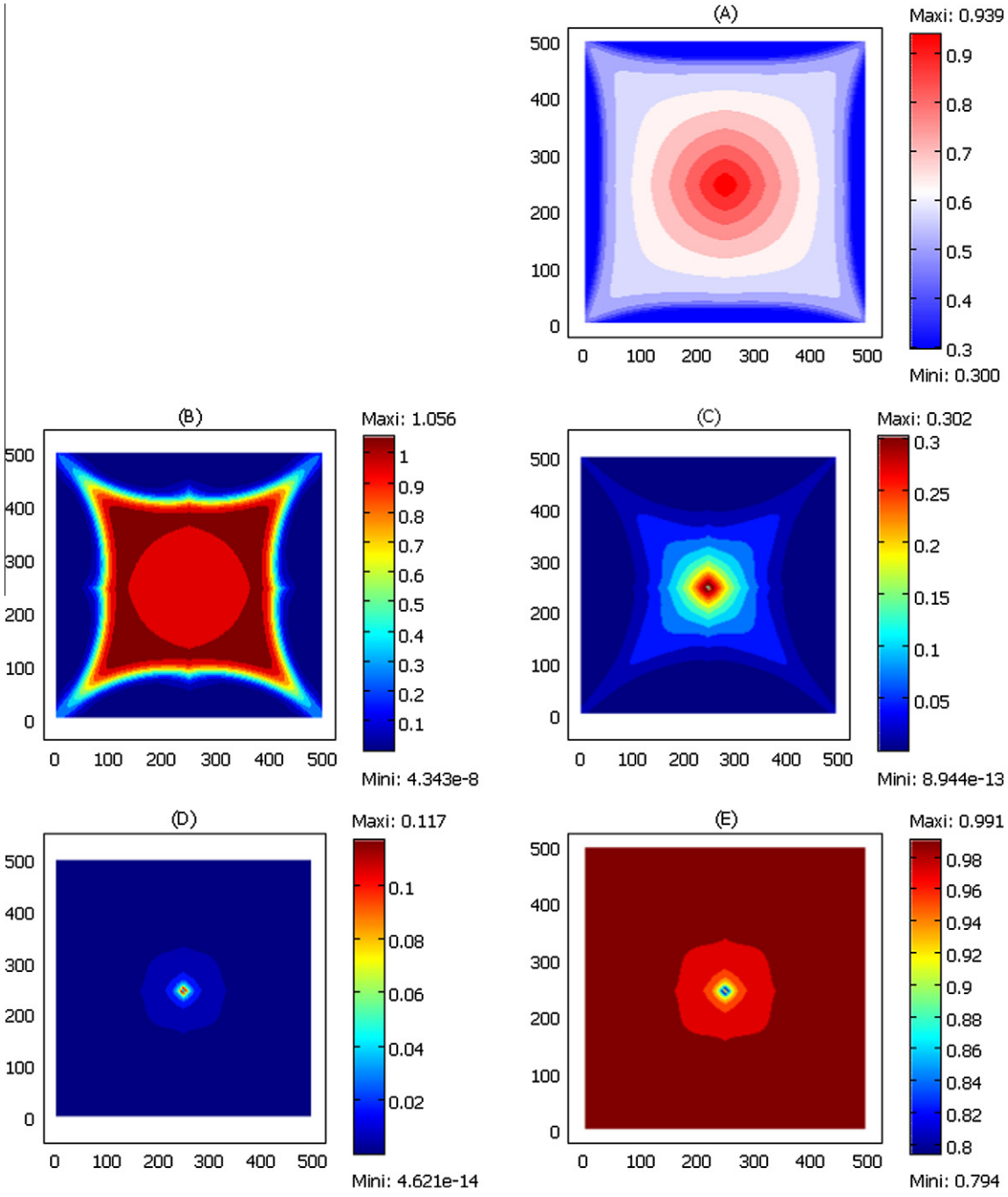

Fig. 9. Simulation results after 1 month of CO_2 injection in a five-spot well pattern – homogeneous medium – $S_{rc} = 0.3$ and $S_{rw} = 0.03$ – showing spatial distribution of (A) CO_2 phase saturation, mass concentrations of (B) suspended particles, (C) deposited particles in pore surfaces, and in (D) pore throats; and (E) the permeability reduction factor.

phase. Such adverse effects could be important for aquifers and flow barriers with a relatively important fraction of clay minerals as they may lead to subtle particulate two-phase flow interactions. Future extensions of the model along this direction are warranted.

Although there are a number of limitations inherent to the complexity of heterogeneous saline aquifers and reservoirs targeted for CO_2 storage, the presented model remains a first step towards a more advanced integration of particle release, mobilization, and capture processes into the framework of other complex CO_2 sequestration numerical models. Examples of new research avenues to this end would be coupling of particulate transport equations with non-isothermal multiphase flow, multicomponent reactive transport, and reservoir compositional models.

6. Summary and concluding remarks

A comprehensive mathematical model of particulate release, migration, and capture in two-phase flow systems is developed. The numerical model procedure is verified on the laboratory scale with available experimental data, and a good agreement with other authors is obtained. This model is useful in field planning of fluids re-injection and production. It is a comprehensive tool to study particulate transport processes for CO_2 injection projects.

CO_2 injection may involve sanding problems on poorly consolidated geological layers which accelerates breakthrough of in situ hydrodynamically released particles. Numerical simulations on a simplified two-dimensional five spots pattern test case highlights

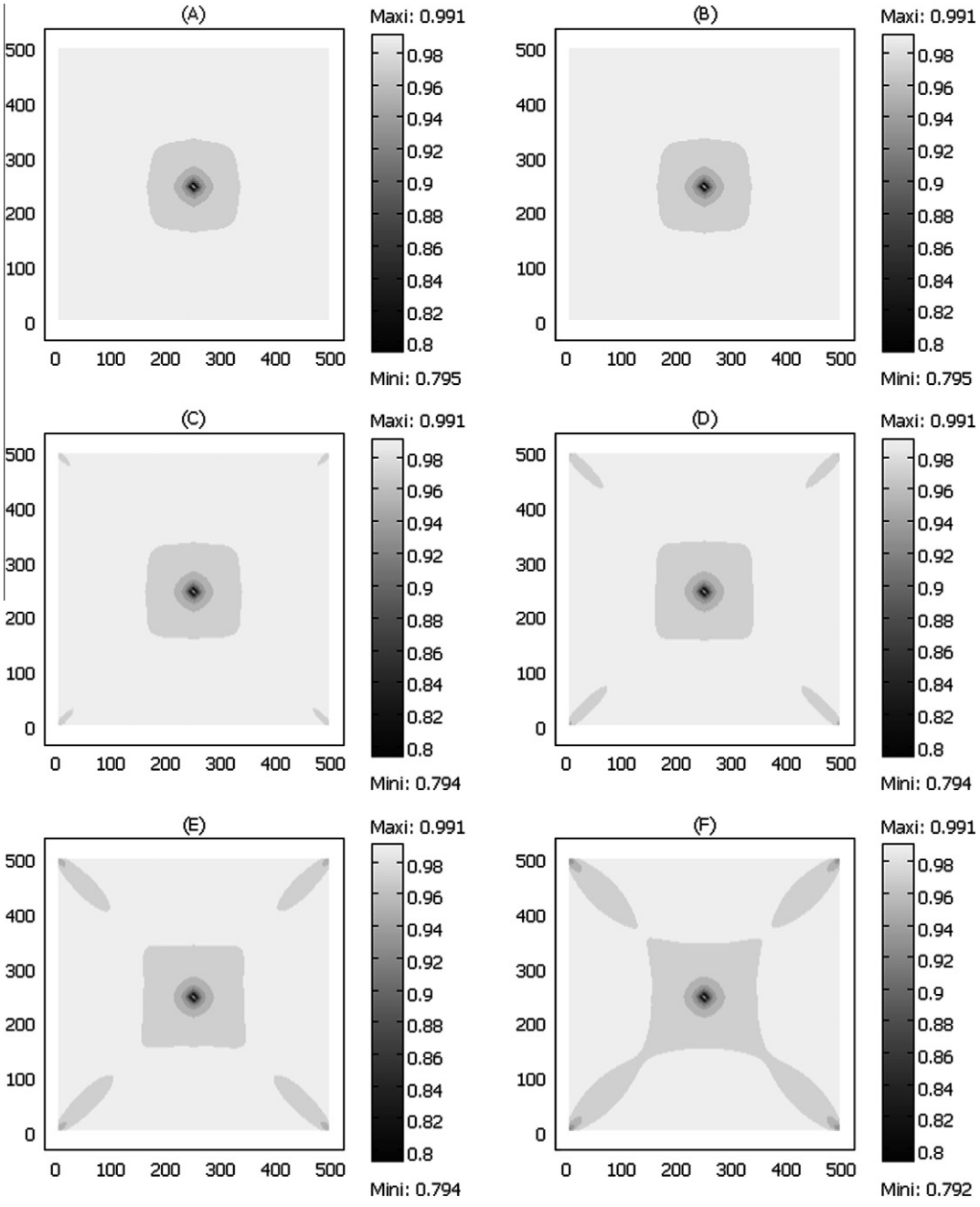

Fig. 10. Simulation results after 1 month of CO_2 injection in a five-spot well pattern – homogeneous medium – $S_{rc} = 0.3$ and $S_{rw} = 0.3$ – showing spatial distribution of the permeability reduction factor for (A) $\phi = 0.35$, (B) $\phi = 0.3$, (C) $\phi = 0.25$, (D) $\phi = 0.2$, (E) $\phi = 0.15$, and (F) $\phi = 0.1$.

Table 5
Parameters used for studying CO_2 injection into two-dimensional heterogeneous layers extracted from SPE-10 comparative solution project.

Parameters of the geological model	Value 365.76	Parameters for fines mobilization	Value
Reservoir length (m)	100	α_{fc}^{cl} (s^{-1})	0.0
Reservoir width (m)	670.56	α_{fc}^{h} (m^{-1})	3.8×10^{-4}
Reservoir thickness	0.61	α_{fc}^{d} (m^{-1})	1.2×10^{-4}
Number of FV cells	60×220	α_{fc}^{pt} (m^{-1})	6.2×10^{-6}
Initial pressure (MPa)	30	$\alpha_{fe,f}$ (m^3/kg)	0.6
Viscosity of CO_2 (mPa s)	0.077	u_{cc} (m/s)	0.2×10^{-4}
Viscosity of oil (mPa s)	300	σ_{fc0} (kg/m^3)	0.0
Residual CO_2 saturation	0.05	ρ_p (kg/m^3)	2500
Residual oil saturation	0.3		
Injection rate of CO_2 (kg/s)	150		
Temperature (°C)	60		
Fluid salinity (g/l)	50		

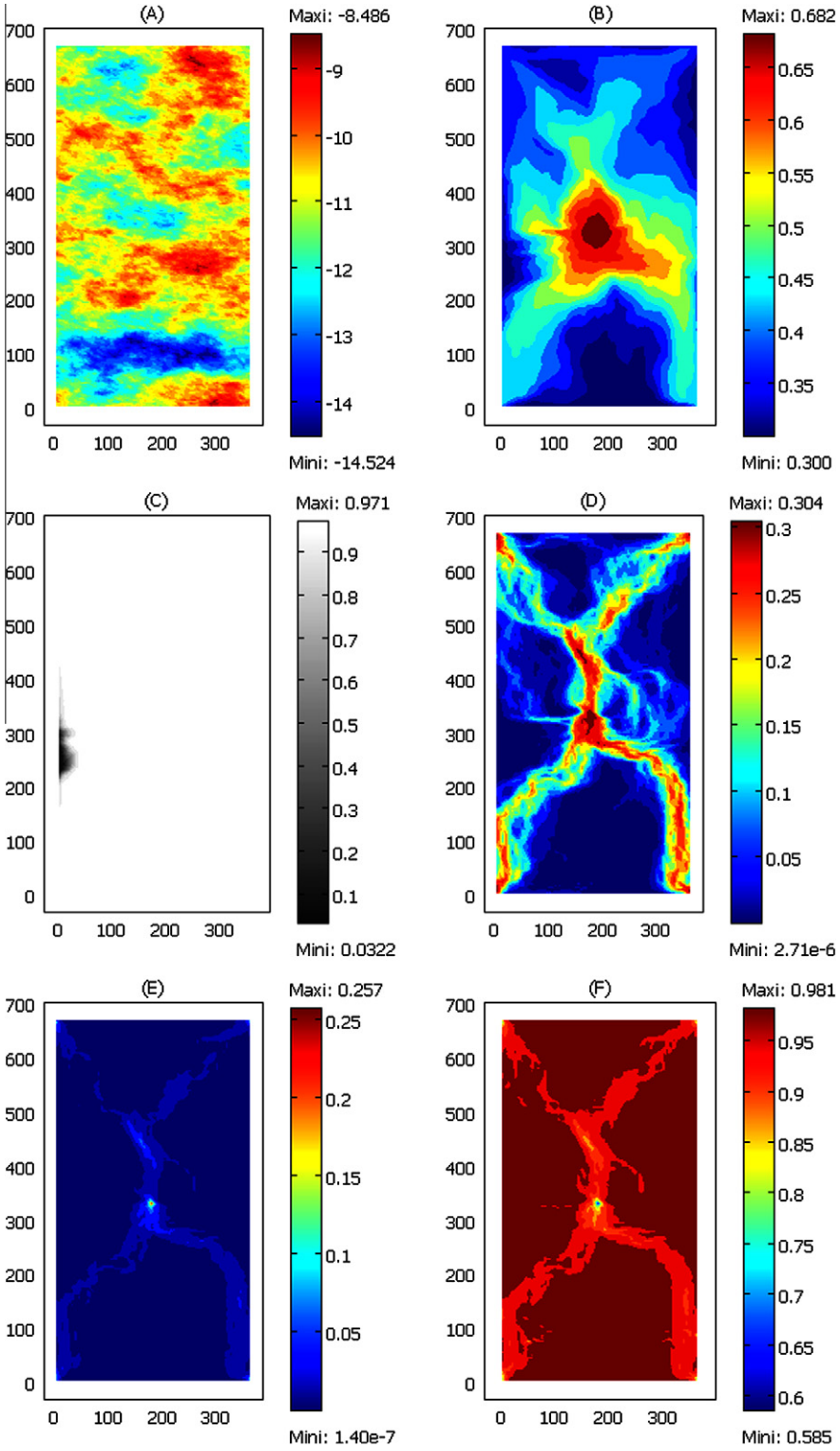

Fig. 11. Simulation results after 1 month of CO_2 injection in a five-spot well pattern – smooth heterogeneous medium case – showing spatial distribution of (A) the initial reservoir permeability (log10-scale) (B) CO_2 phase saturation, mass concentrations of (C) suspended particles, (D) deposited particles in pore surfaces, and in (E) pore throats; and (F) the permeability reduction factor.

the relevance of this processes around the injection and production wells. Under the simple assumption of reservoir homogeneity, lower CO_2 residual saturation and reservoir porosity enhance fines mobility in the reservoir and clogging also around sinks and production wells. The model scope discussed in this paper is limited to the Buckley–Leverett equation with gravity. We expect the same conclusions to hold for if capillary pressure effects are taken into account. Only the magnitude of permeability reduction near the injection well is expected to be different as mobilized and captured particles becomes more diffusive. In the presence of a single injection well like in CO_2 storage the zone of permeability change is expected to be smaller than the case presented in this paper. Due to

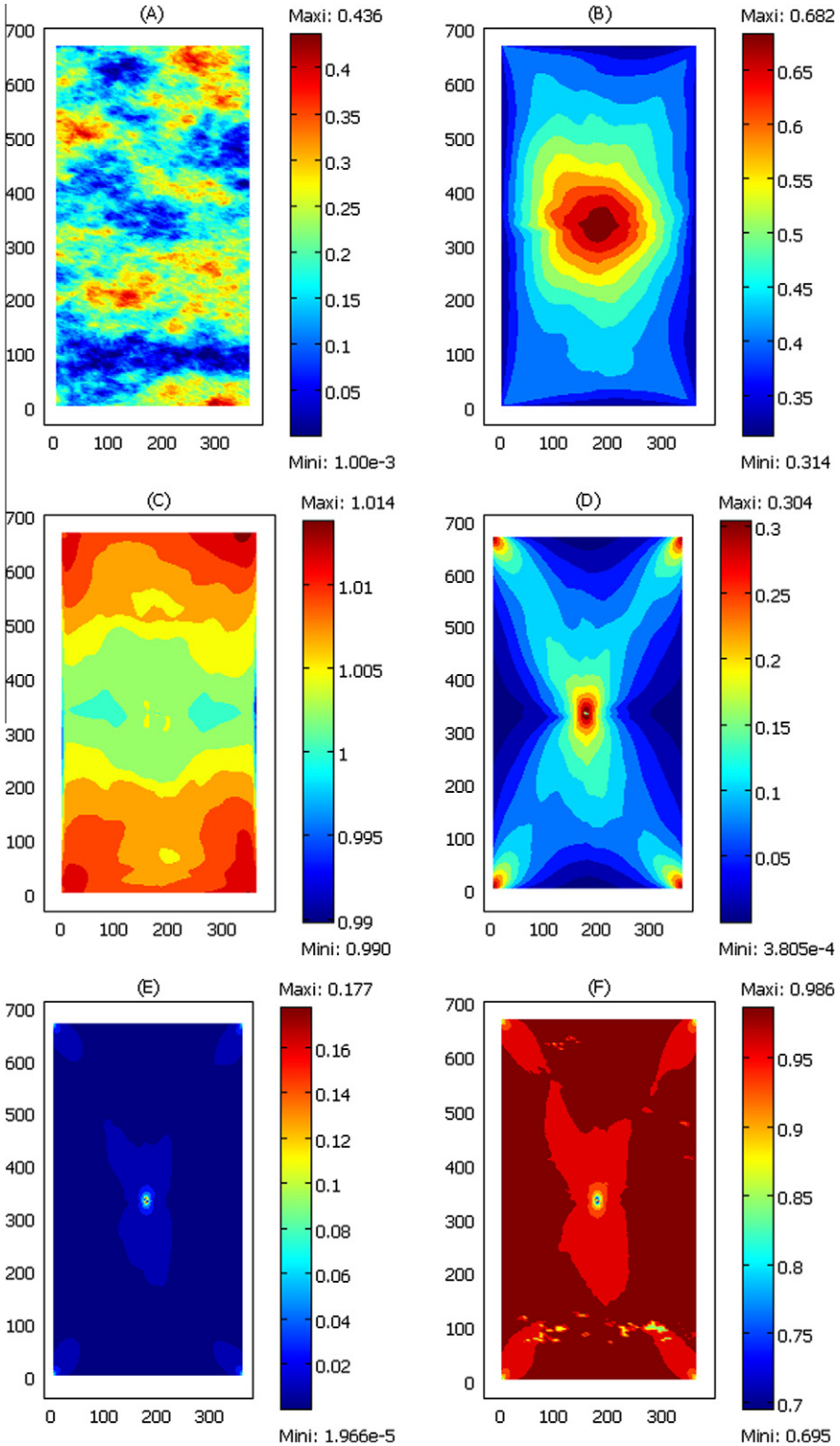

Fig. 12. Simulation results after 1 month of CO_2 injection in a five-spot well pattern – homogeneous mean permeability – showing spatial distribution of (A) the initial reservoir porosity (B) CO_2 phase saturation, mass concentrations of (C) suspended particles, (D) deposited particles in pore surfaces, and in (E) pore throats; and (F) the permeability reduction factor.

the strong buoyancy effects we expect the permeability reduction to be localized in the upper portion of the reservoir beneath the cap rock.

More realistic simulations are performed on several permeability fields, spanning several orders of magnitude, and adapted from the SPE-10 comparative solution project. The results demonstrate that control mode of mobilization, capture, and permeability reduction processes, depends on the type of reservoir heterogeneity such as smoothness, channeling, and connectivity. The clogging process is not limited to the two-dimensional area around the injector and chiefly depends on the type of reservoir heterogeneity. The dimensionality of the problem is another key factor

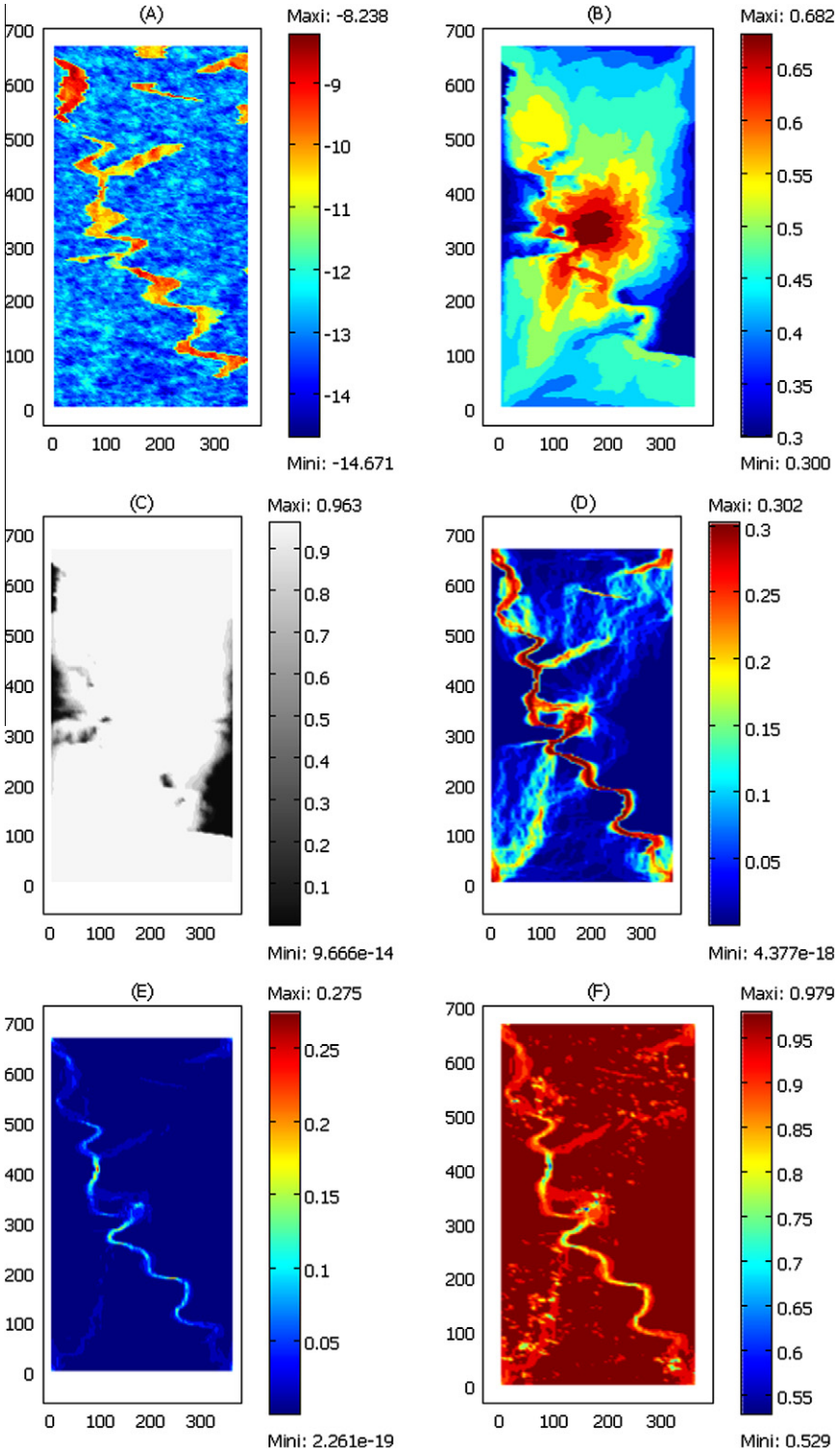

Fig. 13. Simulation results after 1 month of CO_2 injection in a five-spot well pattern – sharp heterogeneous medium case – showing spatial distribution of (A) the initial reservoir permeability (log10-scale) (B) CO_2 phase saturation, mass concentrations of (C) suspended particles, (D) deposited particles in pore surfaces, and in (E) pore throats; and (F) the permeability reduction factor.

implying further improved investigations on three-dimensional problems.

Acknowledgments

We thank the seven anonymous reviewers for their constructive comments which improve the contents and the scope of this paper. This research work was supported by the French Research Agency ANR (Agence Nationale de la Recherche) in the framework of the Geocarbone-Injectivité and Heterogeneites-CO_2 projects.

References

[1] Abdul AS, Gibson TL, Rai DN. Selection of surfactants for the removal of petroleum products from shallow sandy aquifers. Ground Water 1990;28(6):920–6.

[2] Alvarez AC. Inverse problems for deep bed filtration in porous media. PhD Thesis. Brasil: IMPA; 2005.
[3] Alvarez AC, Hime G, Marchesin D, Bedrikovetsky PG. The inverse problem of determining the filtration function and permeability reduction in flow of water with particles in porous media. Transport Porous Med 2005;70:43–62.
[4] Amaziane B, Jurak M. A new formulation of immiscible compressible two-phase flow in porous media. CR Mecanique 2008;336:600–5.
[5] Amirbahman A, Olson TM. Transport of humic matter-coated hematite in packed beds. Environ Sci Technol 1993;27(13):2807–13.
[6] André L, Audigane P, Azaroual M, Menjoz A. Numerical modeling of fluid–rock chemical interactions at the supercritical CO_2-liquid interface during CO_2 injection into a carbonate reservoir, the Dogger aquifer (Paris Basin, France). Energ Convers Manage 2007;48(6):1782–97.
[7] André L, Azaroual M, Menjoz A. Numerical simulations of the thermal impact of supercritical CO_2 injection on chemical reactivity in a carbonate saline reservoir. Transport Porous Med 2010;82:247–74.
[8] Aziz K, Settari A. Petroleum reservoir simulation. Applied Science Publishers; 1979.
[9] Baines SJ, Worden RH, (Eds.), Geological storage of carbon dioxide, London: Geological Society, Special Publications; 2004. p. 233.
[10] Barnes I. Water mineral reactions related to potential fluid injection problems in underground waste management and environment implications. Am Assoc Petr Geol Mem 1972;18:294–7.
[11] Bear J. Dynamics of fluids in porous media. New York: Elsevier; 1972.
[12] Bedrikovetsky PG, Marchesi D, Shecaira F, Souza AL, Milanez PV, Rezende E. Characterization of deep bed filtration system from laboratory pressure drop measurements. J Petrol Sci Eng 2001;32:167–77.
[13] Bennion B, Bachu S. Relative permeability characteristics for supercritical CO_2 displacing water in a variety of potential sequestration zones in the Western Canada sedimentary basin. In: Paper SPE 95547, presented at the 2005 SPE annual technical conference and exhibition, October 9–12, Dallas, TX, USA; 2005.
[14] Bennion B, Bachu S. Dependence on temperature, pressure, and salinity of the IFT and relative permeability displacement characteristics of CO_2 injected in deep saline aquifers. In: Paper SPE 102138, presented at the 2006 SPE annual technical conference and exhibition, September 24–27, San Antonio, TX, USA; 2006.
[15] Benson SM, Tomutsa L, Silin D, Kneafsy T. Core scale and pore scale studies of carbon dioxide migration in saline formations, GHGT-8. Norway: Trondheim; 2006.
[16] Berryman JG, Blair SC. Use of digital image analysis to estimate fluid permeability of porous materials. J Appl Phys 1986;60:1930–8.
[17] Boisdet A, Cautru JP, Czernichowski I. Experiments on reinjection of geothermal brines in deep triassic sandstones. In: Proceedings of the fourth international seminar on the results of EC geothermal energy, Italy; 1989. p. 419–28.
[18] Brown PN, Hindmarsh AC, Petzold LR. Using krylov methods in the solution of large-scale differential-algebraic systems. SIAM J Sci Comput 1994;15:1467–88.
[19] Buckley SE, Leverett MC. Mechanism of fluid displacement in sands. Trans Am Inst Min Met Eng 1942;146:107–16.
[20] Carman P. Fluid flow through a granular bed. Trans Inst Chem Eng 1937;15:150–67.
[21] Chalbaud C, Robin M, Lombard J-M, Martin F, Egermann P, Bertin H. Interfacial tension measurements and wettability evaluation for geological CO_2 storage. Adv Water Resour 2009;22(1):98–109.
[22] Chavent G, Jaffré J. Mathematical models and finite elements for reservoir simulation. Elsevier; 1986.
[23] Chen Z, Huan G, Ma Y. Computational methods for multiphase flows in porous media. Philadelphia: SIAM; 2006.
[24] Christie MA, Blunt MJ. Tenth SPE comparative solution project: a comparison of upscaling techniques. SPE Reserv Eng Eval 2001;4(4):308–17.
[25] Civan F. Reservoir formation damage: fundamentals, modeling, assessment, and mitigation. Elsevier; 2007.
[26] Cui ZD, Wu SL, Li CF, Zhu SL, Yang XJ. Corrosion behavior of oil tube steels under conditions of multiphase flow saturated with super-critical carbon dioxide. Mater Lett 2004;58:1035–40.
[27] Da Silva M, Bedrikovetsky PG, Van der Broek GT, Siqueira A, Serra AL. A new method for injectivity impairment characterization from coreflood and well data, SPE 89885; 2004.
[28] Davis KE, Russel WB. An asymptotic description of transient settling and ultrafiltration of colloidal dispersions. Colloid Surface A 1989;1:82–100.
[29] Degueldre C, Baeyens B, Goerlich W, Riga J, Verbist J, Stadelmann P. Colloids in water from a subsurface fracture in granitic rock, Grimsel Test Site, Switzerland. Geochim Cosmochim Acta 1989;53(3):603–10.
[30] Donaldson ER, Baker BA. Particle transport in sandstones. In: Fifty-second annual fall technical conference and exhibition of the SPE of AIME, Denver CO, USA, SPE 6905, vol. 912; 1977.
[31] Doughty C. Modeling geologic storage of carbon dioxide: comparison of non-hysteretic and hysteretic characteristic curves. Energ Convers Manage 2007;48(6):1768–81.
[32] Dullien FAL. Porous media: fluid transport and pore structure. New York: Academic Press; 1979.
[33] EPA/625/6-89/025a. Kerr RS. Assessing the geochemical fate of deep-well injected hazardous waste: a reference guide. Ada, OK: Environmental Research Laboratory; 1990.
[34] Farajzadeh R. Produced water re-injection (PWRI): an experimental investigation into internal filtration and external cake build up. Report TA/PW/04-14, M.Sc. Thesis. TUDelft: Faculty of Civil Engineering and Geoscience; 2004.
[35] Frydman M. Initiation and propagation of fractures in petroleum wellbores. PhD Thesis. Civil Eng. Dep., PUC-Rio; 1996.
[36] Frydman M, Da Fontoura SAB. Fracturing and progressive plugging simulation during produced water reinjection. In: SPE Latin American and Caribbean petroleum engineering conference, Caracas, SPE 53790; 1999.
[37] Goldenberg LC, Magaritz M, Mandel S. Experimental investigation on irreversible changes of hydraulic conductivity on the seawater–freshwater interface in coastal aquifers. Water Resour Res 1983;19(1):77–85.
[38] Gruesbeck C, Collins RE. Entrainment and deposition of fines particles in porous media. Soc Petrol Eng J 1982:847–56.
[39] Helmig R. Multiphase flow and transport processes in the subsurface. Springer; 1997.
[40] Herzig JP, Leclerc DM, Le Goff P. Flow of suspensions through porous media – application to deep filtration. Ind Eng Chem 1970;62(5):8–35.
[41] Intergovernmental Panel on Climate Change (IPCC). IPCC special report on carbon dioxide capture and storage. New York: Cambridge University Press; 2005.
[42] Iwasaki T. Some notes on sand filtration. J Am Water Works Ass 1937;29(10):1591–602.
[43] Ju BS, Dai SG. A study of wettability and permeability change caused by adsorption of nanometer structured polysilicon on the surface of porous media. In: SPE Asia Pacific oil and gas conference and exhibition, SPE 77938, Melbourne, Australia; 2002. p. 915—26.
[44] Ju B, Fan T, Wang X, Qiu X. A new simulation framework for predicting the onset and effects of fines mobilization. Transport Porous Med 2007;68:265–83.
[45] Kaplan DI, Bertsch PM, Adriano DC, Miller WP. Soil-borne mobile colloids as influenced by water flow and organic carbon. Environ Sci Technol 1993;27(6):1193–200.
[46] Kharaka YK, Cole DR, Hovorka SD, Gunter WD, Knauss KG, Freifeld BM. Gas water rock interactions in Frio Formation following CO_2 injection: implications for the storage of greenhouse gases in sedimentary basins. Geology 2006;34:577–80.
[47] Khilar KC, Fogler HS. Water sensitivity of sandstones. Soc Petrol Eng J 1983: 55–64.
[48] Kwok F, Tchelepi HA. Potential-based reduced newton algorithm for nonlinear multiphase flow in porous media. J Comput Phys 2007;227(1):706–27.
[49] Kozeny J. Uber kapillare leitung der wasser in boden, Sitzungsber. Akad Wiss Wien 1927;136:271–306.
[50] Ku CA, Henry Jr JD. Mechanisms of particle transfer from a continuous oil to a dispersed water phase. J Colloid Interf Sci 1987;116(2):414–22.
[51] Leroy Ph, Lassin A, Azaroual M, André L. Predicting the surface tension of aqueous 1–1 electrolyte solutions. Geochim. Cosmochim. Acta 2010;74(19): 5427–42.
[52] LeVeque RJ. Numerical methods for conservation laws. Zurich: Birkhauser; 1992.
[53] Liu X, Civan F. Characterization and prediction of formation damage in two-phase flow systems, SPE 25429; 1993.
[54] McDowell-Boyer LM, Hunt JR, Sitar N. Particle transport through porous media. Water Resour Res 1986;22:1901–21.
[55] Moghadasi J, Steinhagen HM, Jamialahmadi M, Sharif A. Theoretical and experimental study of particle movement and deposition in porous media during water injection. J Petrol Sci Eng 2004;43:163–81.
[56] Moore J, Adams M, Allis R, Lutz S, Rauzi S. Mineralogical and geochemical consequences of the long-term presence of CO_2 in natural reservoirs: an example from the Springerville St. Johns Field, Arizona, and New Mexico, USA. Chem Geol 2005;217(3–4):365–85.
[57] Muecke TW. Formation fines and factors controlling their movement in porous media. J Petrol Technol 1979:144–50.
[58] Nasr-El-Din HA, Al-Mohammad AM, Al-Shurei AA, Merwat NK, Erbil MM, Samuel M. Restoring the injectivity of water disposal wells using a viscoelastic surfactant-based acid. J Petrol Sci Eng 2006;54(1–2):10–24.
[59] Noiriel C, Bernard D, Gouze Ph, Thibault X. Hydraulic properties and microgeometry evolution accompanying limestone dissolution by acidic water. Oil Gas Sci Technol 2005;60(1):177–92.
[60] Ochi J, Vernoux J-F. Permeability decrease in sandstone reservoirs by fluid injection: hydrodynamic and chemical effects. J Hydrol 1998;208(3–4):237–48.
[61] Ochi J, Vernoux J-F. A Two-dimensional network model to simulate permeability decrease under hydrodynamic effect of particle release and capture. Transport Porous Med 1999;37:303–25.
[62] Pang S, Sharma MM. A model for predicting injectivity decline in water injection wells, SPE 28489; 1994.
[63] Pang S, Sharma MM. Evaluating the performance of open-hole, perforated and fractured water injection wells, SPE 30127; 1995.
[64] Paniconi C, Putti M. A comparison of Picard and Newton iteration in the numerical solution of multidimensional variably saturated flow problems. Water Resour Res 1994;30(12):3357–74.
[65] Peaceman DW. Interpretation of well-block pressures in numerical reservoir simulation with nonsquare gridblocks and anisotropic permeability. Soc Petrol Eng J 1983;23(3):531–43.
[66] Perrin J-C, Benson SM. An experimental study on the influence of sub-core scale heterogeneities on CO_2 distribution in reservoir rocks. Transport Porous Med 2009. doi:10.1007/s11242-009-9426-x.

[67] Petsev DN, Starov VM, Ivanov IB. Concentrated dispersions of charged colloidal particles. Colloid Surface A 1993;81:65–81.
[68] Pruess K, Muller N. Formation dry-out from CO_2 injection into saline aquifers: 1. Effects of solids precipitation and their mitigation. Water Resour Res 2009;45:W03402.
[69] Ryan JN, Gschwend PM. Effect of iron diagenesis on the transport of colloidal clay in an unconfined sand aquifer. Geochim Cosmochim Acta 1992;56(4):1507–21.
[70] Saripalli KP, Sharma MM, Bryant SL. Modeling the injection well performance during deep-well injection of liquid wastes. J Hydrol 2000;227:41–55.
[71] Sarkar AK. An experimental investigation of fines migration in two phase flow. M.S. Thesis. University of Texas at Austin; 1988.
[72] K Sarkar A, Sharma MM. Fines migration in two-phase flow. J Petrol Technol 1990:646–52.
[73] Sarkar AK, Georgiou G, Sharma MM. Transport of bacteria in porous media, part 1. An experimental investigation. Biotechnol Bioeng J 1994;44(4):489–97.
[74] Sarkar AK, Georgiou G, Sharma MM. Transport of bacteria in porous media, part 2. A model for convective transport and growth. Biotechnol Bioeng J 1994;44(4):498–507.
[75] Schlueter EM. Predicting the transport properties of sedimentary rocks from microstructure. PhD Thesis. Berkeley: University of California; 1995.
[76] Shao H, Ray JR, Jun Y-S. Dissolution and precipitation of clay minerals under geologic CO_2 sequestration conditions: CO_2-brine-phlogopite interactions. Environ Sci Technol 2010;44(15):5999–6005.
[77] Sharma MM, Yortsos YC. Fines migration in porous media. AIChE J 1987;33(10):1654–62.
[78] Sharma MM, Yortsos YC. A network model for deep bed filtration processes. AIChE 1987;33(10):1644–53.
[79] Sharma MM, Pang S, Wennberg KE, Morgenthaler LN. Injectivity decline in water injection wells: an offshore Gulf of Mexico case study. SPE Prod Facil J 2000;15:6–13.
[80] Suarez DL, Rhoades JD, Lavado R, Grieve CM. Effect of pH on saturated hydraulic conductivity and soil dispersion. Soil Sci Soc Am J 1984;48:50–5.
[81] Tufenkji N, Redman JA, Elimelech M. Interpreting deposition patterns of microbial particles in laboratory-scale column experiments. Environ Sci Technol J 2003;37:616–23.
[82] Tufenkji N. Modeling microbial transport in porous media: traditional approaches and recent developments. Adv Water Res 2007;30:1455–69.
[83] Van der Broek GT, Bruin JN, Tran TK, Van der Zande MJ, Van der Meulen H. Core-flow experiments with oil and solids containing water. In: SPE European formation damage conference, 31 May – 1 June, The Hague, The Netherlands, SPE 54769; 1999.
[84] Van Velzen JFG, Leerlooijer K. Impairment of a water injection well by suspended solids: testing and prediction. In: SPE international symposium on formation damage control, Lafayette, LA, SPE 23822; 1992.
[85] Van Oort E, Van Velzen JFG, Leerlooijer K. Impairment by suspended solids invasion: testing and prediction. SPE Prod Facil J 1993:178–84.
[86] Valvatne PH, Piri M, Lopez X, Blunt MJ. Predictive pore-scale modeling of single and multiphase flow. Transport Porous Med 2005;58:23–41.
[87] Verma A, Pruess K. Thermohydrological conditions and silica redistribution near high-level nuclear wastes emplaced in saturated geological formations. J Geophys Res 1988;93:1159–73.
[88] Weissberg HL. Effective diffusion coefficient in porous media. J Appl Phys 1963;34:26–36.
[89] Wennberg KE. Particle retention in porous media: application to water injectivity decline. PhD Thesis. Trondheim: Norwegian University of Science and Technology; 1998, p. 177.
[90] Wojtanowicz AK, Krilov Z, Langlinais JP. Study on the effect of pore blocking mechanisms on formation damage. In: SPE production operations symposium, March 8–10, Oklahoma City, OK, USA, SPE 16233; 1987.
[91] Yamamoto T, Fujishima H, Okubo M, Kuroki T. Pilot-scale NO_x and SO_x removal from boiler emission using radical injection and chemical hybrid process. In: Paper 2C1 presented in ICESP X, Australia; 2006.